KNEE ANGLE AND AXES CROSSTALK CORRECTION IN GAIT, CYCLING, AND ELLIPTICAL TRAINING EXERCISES

A Thesis

presented to

the Faculty of California Polytechnic State University,

San Luis Obispo

In Partial Fulfillment

of the Requirements for the Degree

Master of Science in Mechanical Engineering

by

Jordan Skaro

May 2018

COMMITTEE MEMBERSHIP

TITLE:	Knee Angle and Axes Crosstalk Correction in Gait, Bicycling, and Elliptical Training Exercises
AUTHOR:	Jordan Skaro
DATE SUBMITTED:	May 2018
COMMITTEE CHAIR:	Stephen Klisch, Ph. D. Professor of Mechanical Engineering
COMMITTEE MEMBER:	Scott Hazelwood, Ph. D. Professor of Biomedical Engineering
COMMITTEE MEMBER:	James Widmann, Ph. D. Professor of Mechanical Engineering

ABSTRACT

Knee Angle and Axes Crosstalk Correction in Gait, Bicycling, and Elliptical Training Exercises

Jordan Skaro

When conducting motion analysis using 3-dimensional motion capture technology, errors in marker placement on the knee results in a widely observed phenomenon known as “crosstalk” [1-18] in calculated knee joint angles (i.e., flexion-extension (FE), adduction-abduction (AA), internal-external rotation (IE)). Principal Component Analysis (PCA) has recently been proposed as a post hoc method to reduce crosstalk errors and operates by minimizing the correlation between the knee angles [1, 2]. However, recent studies that have used PCA have neither considered exercises, such as cycling (C) and elliptical training (E), other than gait (G) nor estimated the corrected knee axes following PCA correction. The hypothesis of this study is that PCA can correct for crosstalk in G, C, and E exercises but that subject-specific PCA corrected axes differ for these exercises.

Motion analysis of the selected exercises were conducted on 8 normal weight (body mass index (BMI) = 21.70 +/- 3.20) and 7 overweight participants (BMI = 27.45 +/- 2.45). An enhanced Helen Hayes marker set with 27 markers was used to track kinematics. Knee joint FE, AA, and IE angles were obtained with Cortex (Motion Analysis, Santa Rosa, CA) software and corrected using PCA to obtain corrected angles for each exercise. Exercise-specific corrected knee joint axes were determined by finding axes that reproduced the shank and ankle body vectors taken from Cortex when used with the PCA corrected angles. Then, PCA corrected gait axes were used as a common set of axes for all exercises to find corresponding knee angles. Paired t-tests assessed if FE-AA angle correlations changed with PCA. Multivariate Paired Hotelling’s T-Square tests assessed if the PCA corrected knee joint axes were similar between exercises. ANOVA was used to assess if Cortex angles, PCA corrected angles, and knee angles using PCA corrected gait axes were different.

Reduced FE-AA angle correlations existed for G ($p<0.001$ for Cortex and $p=0.85$ for PCA corrected), C ($p=0.01$ for Cortex and $p=0.77$ for PCA corrected), and E ($p<0.001$ for Cortex and $p=0.77$ for PCA corrected). Differences in the PCA corrected knee axes were found between G and C ($p<0.0014$). Then, differences were found between Cortex, PCA corrected, and C and E knee angles using the PCA corrected G axes ($p<0.0056$).

The results of this study suggest that if PCA is used to reduce crosstalk errors in motions other than G then it is recommended to adopt the use of a PCA corrected axes set determined from G to produce the PCA corrected angles.

Keywords: PCA, crosstalk, biomechanics, knee angles, knee axes, gait, cycling, elliptical training

ACKNOWLEDGMENTS

This work was supported by the W.M. Keck Foundation, the Donald E. Bently Center, and by the Defense Health Program, through the Department of Defense Broad Agency Announcement for Extramural Medical Research Program Number W81XWH-BAA-14-1under Award No. W81XWH-16-1-0051. Opinions, interpretations, conclusions and recommendations are those of the author and are not necessarily endorsed by the Department of Defense. We thank Dr. Jeffrey Sklar of California Polytechnic State University for being an excellent resource on statistical methods.

TABLE OF CONTENTS

Page

LIST OF TABLES

LIST OF FIGURES

Chapter 1

INTRODUCTION

Accurate measurement of knee joint kinematics has numerous important clinical applications. Motion analysis using 3-dimensional (3D) motion capture technology provides critical information used to evaluate knee motion during activities. Clinical analyses rely on this information for pre- and post-intervention assessments of patient dynamic functionality [19-22]. Other assessment methods can be used, such as visual analysis, physical examination, and static magnetic resonance imaging (MRI), but the accuracy is limited by the examiner, MRI resolution, and how the analyses are interpreted. Precise results are desired for patients that potentially have tibial or femoral torsion, inward twisting of the shin and thigh bones, respectively, where the lower extremity kinematics play an important role in the surgeon's decision for de-rotation osteotomy [23-25]. Consequently, surgeons commonly refer to gait (G) analysis to determine if surgery is necessary to create neutral alignment of the lower extremity during stance phase and to reduce off-axis loading of the knee in children with cerebral palsy, patellofemoral instability, and Osgood-Schlatter disease [26, 27]. There is evidence that revisional surgeries are often required which are physically demanding of the patient [28, 29].

Accurately measuring knee axes and kinematics has proved to be difficult [30, 31]. Eulerian or Cardan angle systems are typically used to describe knee joint kinematics [32]. Describing 3D knee joint kinematics requires two body segment coordinate systems (CSs), one for the femur and another for the tibia, and a third joint CS. The body segment CSs are defined by placing retroreflective markers on the surface of the skin on specific lower extremity bony landmarks following a standardized marker set [3, 33-36]. Knee joint kinematics which are calculated from the trajectory of the markers is commonly reported as three sequential rotations (Euler angles) about three distinct axes of the joint CS: flexion-extension (FE), abduction-adduction (AA), and internal-external rotation (IE) [37]. To place these markers, experimenters must palpate the bony landmarks which can introduce experimental errors [38]. This is a significant limitation due to the fact that experiments are performed by researchers with varying methods and skill levels. Marker misplacement has been identified as the largest source of between-laboratory and within-laboratory kinematic variability resulting in up to 75% of the

variance between laboratories [39, 40]. Inconsistent marker placements around the knee also modify the joint CS definition which yields significant errors and an overestimation of the AA and IE rotation angles throughout a variety of activities [4-6, 34, 41-43]. The latter error is commonly known as the kinematic “crosstalk” effect [7, 8, 44, 45] and affects the kinematics of joints that undergo relatively large rotations about one major axis [9], specifically the FE rotations of the knee joint in G. Thus, misplacement of these markers and crosstalk lead to incorrect results for the knee joint axes and angles, respectively.

Crosstalk develops from misplacement of the markers which define the joint CS during motion capture experiments. This is analogous to the motion perceived of a ball by the two people playing and by someone watching in a simplified 2D case shown in Figure 1.1. Person 1 and 2 playing catch would perceive the motion of the ball primarily in the X-direction because their CS is set as such by their vision. While Person 3, standing askew to the ball path, would perceive the ball being thrown in both the X’- and Y’-directions because their CS set by their vision is defined askew to the ball path. Notice in the second case, the path of the ball is the same but distributed differently among the X-Y and X’-Y’-directions. Also, if the ball was thrown further, the X’ component of the ball trajectory would increase with the Y’ component, creating a correlation between the X’ and Y’ components of the ball trajectory.

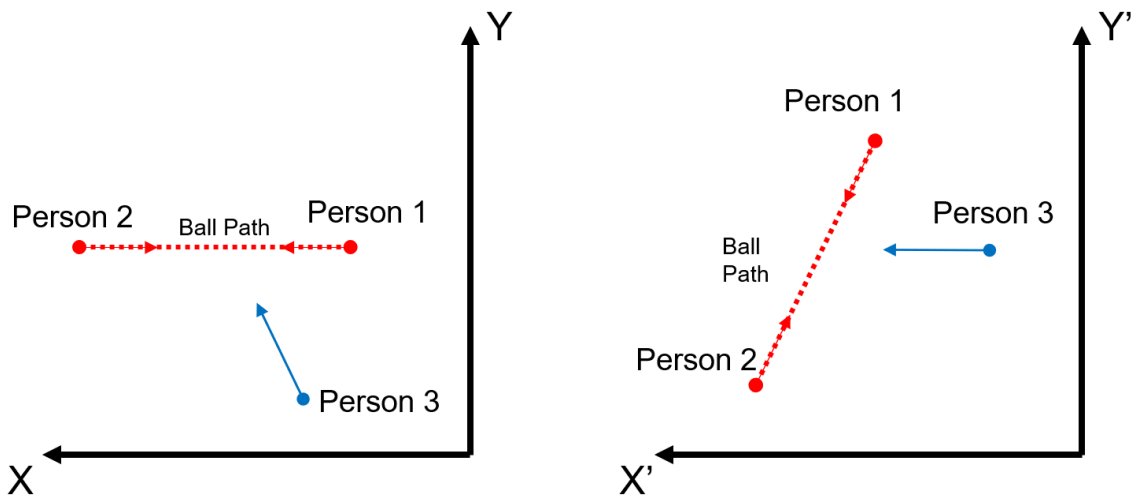

Figure 1.1: A diagram of the ball throwing example. Left diagram displays the ball motion when the CS is aligned with Person 1 and 2's perspective. Right diagram displays the ball motion when the CS is aligned with Person 3's perspective.

In the case of joint motion, FE is the primary rotation of the knee joint, thus it should behave similar to the ball motion perceived by Person 1 and 2. Though, if incorrect marker placement skews the CS of the knee, then it will cause knee motion to be interpreted as Person 3. This will cause shank motion to be interpreted as FE and AA instead of primarily FE and there will be a correlation between FE and AA. This can be visualized using a simple case of knee flexion while sitting with minimal shank IE rotation (Figure 1.2). Sitting while flexing and extending your knee, the motion would be expected to be predominantly FE. It can be seen that if there is slight marker misplacement and joint CS mis definition then some of the motion would be misinterpreted as AA to allow the shank to complete its observed trajectory. In a case of severe marker misplacement, AA is misinterpreted for a larger portion of the shank's motion. In both of these cases, AA will increase proportionality to FE and, thus, will create a correlation between FE and AA. Correcting crosstalk in the ball and knee flexion example would require rotating the CS to allow the trajectory to again be primarily in the x and FE components, respectively. This is the most correct way to interpret knee motion.

By not correcting the knee angles and axes for crosstalk to get accurate results, inappropriate pre- and post-intervention assessments of patient dynamic functionality may be performed. This may lead to inappropriate surgical interventions with the purpose of creating neutral alignment of the knee in children with cerebral palsy, patellofemoral instability, and Osgood-Schlatter disease. By increasing the efficiency for these surgical interventions, the physical and financial demand of the patient would be minimized.

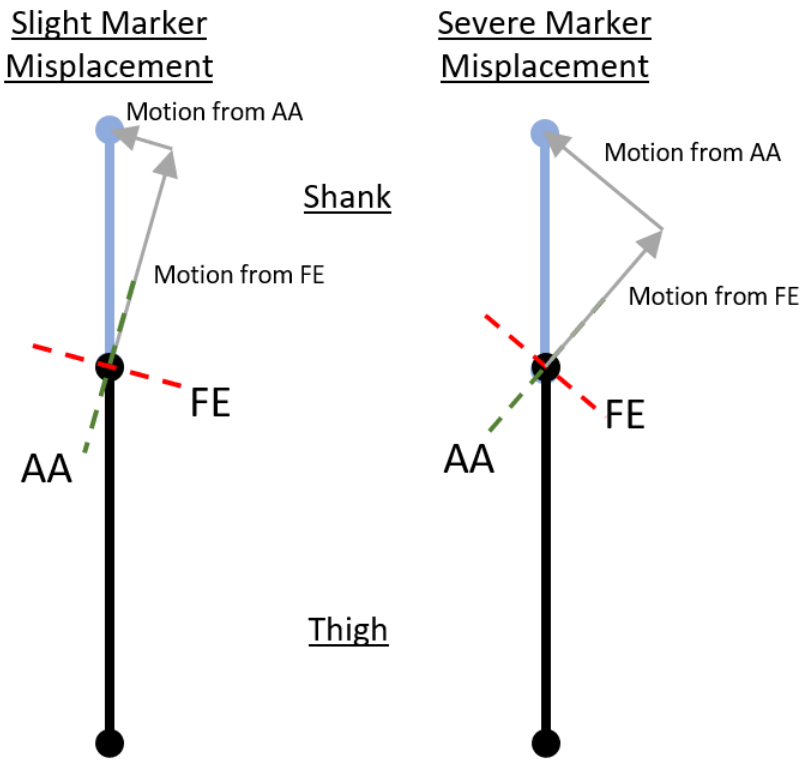

Figure 1.2: A simplified 2D model describing the impact crosstalk and joint CS definition have on the angles reported from motion capture analysis with two scenarios. One scenario with slight crosstalk due to slight marker misplacement and a second with severe crosstalk due to severe marker misplacement. The model can be visualized as sitting with the thigh fixed while swinging the shank through a normal range of motion.

Several other methods have been studied to reduce crosstalk errors [10-17, 46-48]. Some of those methods are implemented as a post hoc technique to identify the functional knee

axes using range-of-motion trials such as squats or passive knee flexion prior to data collection [15, 46]. The functional knee axes were then used to determine the knee kinematics instead of relying on knee axes defined by marker placement. Though those techniques are less susceptible to the human error encountered during marker placement they are limited by the patient's physical ability. If the patient is physically-impaired, they might not be able to accomplish these trials and continue through the experiment. One study eliminates crosstalk in the knee angles by altering the joint CS to zero AA and IE at maximum knee FE and minimizing the quadratic variations in knee AA and IE angles [16, 17]. While that technique has been shown to reduce crosstalk, it may also eliminate important existing mechanisms of the knee joint. In another study, an algorithm is implemented that utilizes standard walking trials to identify the true knee joint axes and has shown to be successful in reducing crosstalk [10, 13]. The algorithm operated by minimizing the knee AA angles to correct the knee flexion axis after data collection. In direct comparison studies, the knee AA minimization method was shown to reduce kinematic errors [10, 13] and matched ultrasound measurements of tibial torsion in healthy subjects [49]. Despite being successful, this algorithm identifies the true knee axes using iterative guessing rather than the more efficient statistical optimization. That method is also ineffective at finding the true knee axes in populations with large AA motion during gait.

More recently, a post hoc correction method has been studied which uses PCA to correct for crosstalk [1, 2] and has shown to be less susceptible to marker placement errors than a null space algorithm [46] and comparable to a knee AA minimization algorithm [10]. Implementing PCA requires no hardware setup which reduces the required time for experiments and utilizes a computationally efficient statistical algorithm that is available to anyone. This study addresses two limitations of previous studies that have used PCA to reduce crosstalk errors. First, previous studies that have used PCA have focused on reducing crosstalk errors as evidenced by reduced FE-AA correlations [1, 2] only in G studies and have not considered whether PCA is effective in reducing crosstalk errors for other exercises such as cycling (C) and elliptical training (E). Second, previous studies that used PCA have not calculated the corrected knee axes corresponding to the PCA corrected knee angles via statistical optimization [8]. C and E exercises

tend to produce higher flexion angles than in G and there may be a natural correlation between FE and AA angles seen at higher flexion angles [50-52]. Thus, PCA may not be appropriate for C and E, and different PCA corrected knee axes may be expected for G, C, and E exercises.

The goals of this study were to 1) assess and compare the ability of PCA to reduce crosstalk errors for three types of exercises with differing knee kinematics: G, C, and E and 2) develop a protocol and algorithm that determines a common set of subject-specific knee axes from PCA corrected gait axes for determining PCA corrected knee angles for multiple exercises. To address the first goal, the first hypothesis was that PCA reduces correlations, an indicator of crosstalk, between knee FE and AA angles in G, C, and E exercises. To address the second goal, a second hypothesis is that the corrected and subject-specific FE and AA axes produced by PCA are different for G, C, and E. To address these hypotheses, the specific aims of this study were to 1) conduct motion analysis experiments with participants tested in G, C, and E experiments and process marker data in Cortex analysis software (Motion Analysis, Santa Rosa, CA, USA) to obtain Cortex knee angles and further post-process marker data with PCA to obtain PCA corrected knee angles, 2) obtain PCA corrected axes from PCA corrected angles via statistical optimization, and 3) propose a common set of axes from the G PCA corrected axes to determine new PCA corrected angles in C and E. Statistical analyses were performed to compare: FE-AA correlations in Cortex and PCA corrected angles; the PCA corrected axes in G, C, and E; and the C and E knee angles from Cortex, PCA-correction, and PCA-correction with a common set of knee axes.

Chapter 2

METHODS

Subject Selection and Informed Consent

Protocols for this study were approved by Cal Poly's Human Subjects Committee and were designed to minimize risk to human subjects. Nine male and six female participants volunteered for this study. Of the 15 subjects, eight were normal weight and seven were overweight, as defined by body mass index (BMI) [53]. Exclusion criteria included obesity, evidence of pre-existing conditions that may produce abnormal knee biomechanics (e.g. varus-valgus misalignment, ligament injuries), and history of cardiovascular, respiratory, or metabolic diseases or complications. Each participant visited the Cal Poly HMB Lab where the study was explained in detail. Each participant was administered a Physical Activity Readiness Questionnaire (PAR-Q) to screen for their ability to engage in exercise and was asked questions pertaining to body weight, body height, and medical history to screen for eligibility. Once eligibility was confirmed informed consent was obtained.

Experiments

The participant completed a warm-up exercise (minimum of 5 minutes) and then changed into compression clothing. Then, 32 retroreflective markers were placed on anatomical landmarks (Top. Head, Front. Head, Rear. Head, R. Acromion, L. Acromion, C7, Sternum, R. ASIS, L. ASIS, R. PSIS, L. PSIS, V. Sacral, R. Thigh, L. Thigh, R. Knee, L. Knee, R. Fibula, L. Fibula, R. Tibial Tuberosity, L. Tibial Tuberosity, R. Shank, L. Shank, R. Ankle, L. Ankle, R. Heel, L. Heel, R. Toe, L. Toe, R. Knee Medial, L. Knee Medial, R. Knee Medial, L. Knee Medial) based on an enhanced Helen Hayes marker set. The participant stood in the center of the room to perform a static pose to calculate lower extremity joint centers and reference joint kinematics (Figures 2.1 – 2.2). After the static pose capture, medial lower extremity markers were removed.

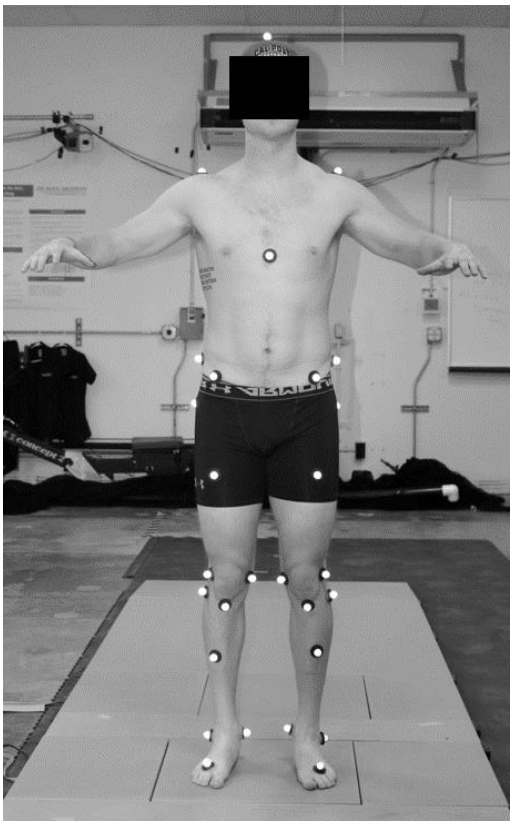

Figure 2.1: Participant performing a static pose, used to calculate knee and ankle joint centers and static joint reference configuration. Markers shown are based on an enhanced Helen Hayes markerset protocol.

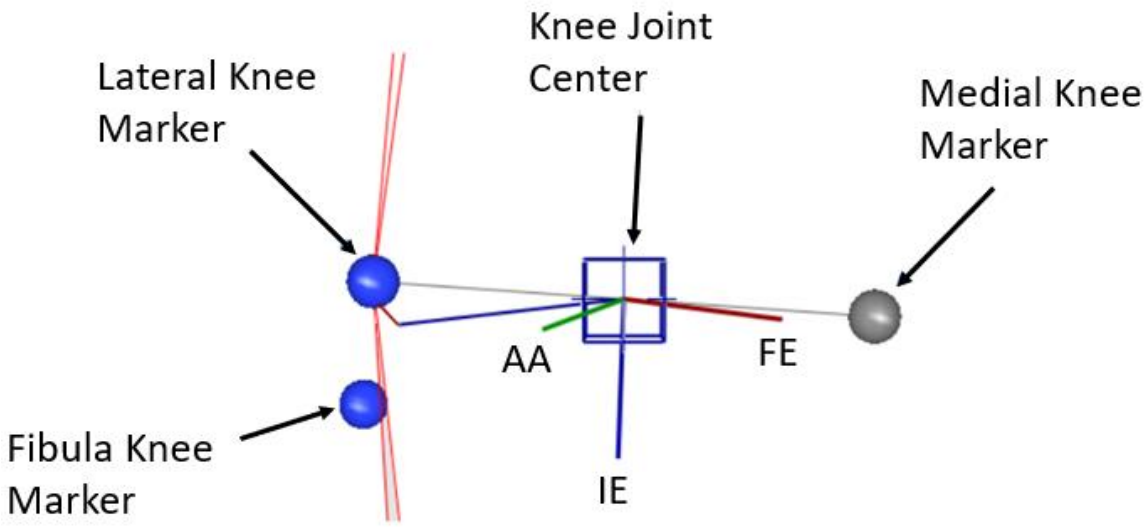

Figure 2.2: The Cortex knee coordinate system and knee joint center.

The HMB Lab includes a motion analysis system with Cortex analysis software and 12 (six Owl, three Osprey, two Kestrel, one Eagle) digital cameras (Motion Analysis, Santa Rosa, CA, USA), used to track retroreflective markers and characterize motion kinematics. For G experiments, the participant walked across four ground force plates (AccuGait, AMTI, Watertown, MA, USA) that measured the time-dependent 3D force and 3D moment vectors. For C experiments, the participant pedaled a stationary bicycle (LifeCycle GX, LifeFitness, Rosemont, IL, USA) with custom pedals each instrumented with one 6-axis load cells (AD2.5D-250, AMTI, Watertown, MA). For E experiments, the participant pedaled an elliptical machine (XE795, Spirit Fitness, Jonesboro, AZ, USA) with custom pedals each instrumented with two 6-axis load cells (AD2.5D-250, AMTI, Watertown, MA) (Figure 2.3).

Figure 2.3: (Left) A participant walking along the walkway during a gait experiment, with the right foot contacting 1 of 3 ground force plates with motion analysis cameras recording G (two cameras are visible to the left and right of the participant's head in left photo). (Middle) pedaling the stationary bike instrumented with load cells on each pedal with markers tracking the pedal orientation. (Right) pedaling the elliptical instrumented with load cells on each pedal.

Marker trajectory was recorded in Cortex analysis software (Version 7.01, Motion Analysis) at 150 Hz and filtered using a 4^{th} order Butterworth filter with a cutoff frequency of 8 Hz for G and 6 Hz for C and E. For G, the participants walked at their preferred walking speed. During C and E testing, the participants pedaled at a cadence of 70 revolutions per minute (RPM) at moderate machine resistance levels (levels 15 and 10 for C and E, respectively). After a warm-up trial for each test, the participants repeated each test until three successful motion studies were captured.

Analysis

Kinematic

For each exercise, kinematic variables FE, AA, and IE angles were collected from three trials and interpolated to 101 time points to reflect a full cycle from 0 to 100 percent. Dynamic angles were defined relative to a reference configuration where the shank was parallel to the thigh. A full G cycle was defined from initial heel strike (0%) to the next heel strike (100%) of the analyzed leg (Figure 2.4). A full C cycle was defined from top dead center (TDC) (0%) to the next TDC (100%) of the analyzed leg (Figure 2.5) [54]. A full E cycle is defined from the furthest forward pedal position (0%) to the next time at the forward pedal position (100%) (Figure 2.6). A custom algorithm was developed (MATLAB, MathWorks, Natick, MA, USA) to perform the data interpolation.

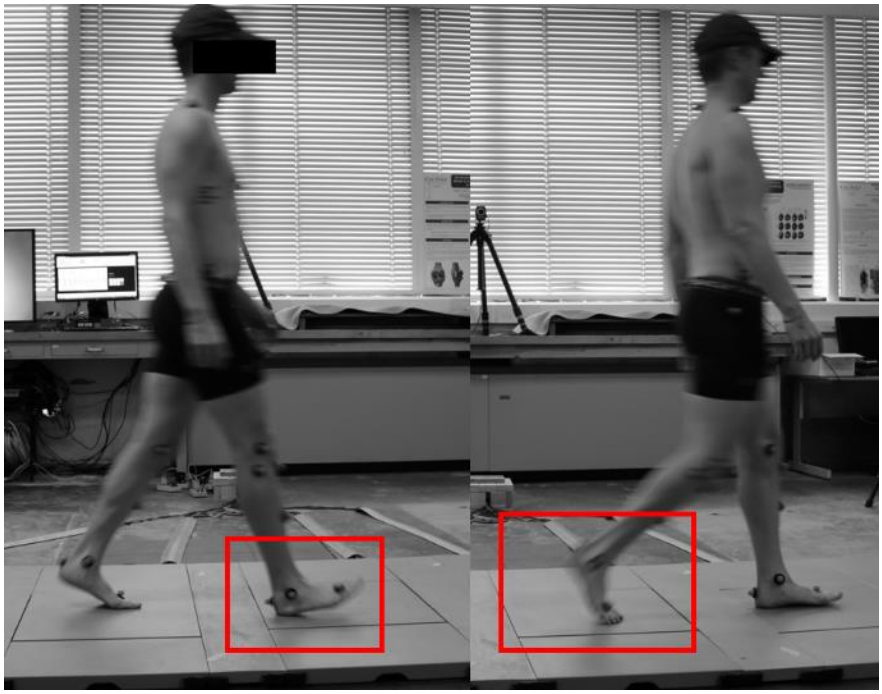

Figure 2.4: Heel strike (left) and toe off (right) which initiate the stance and swing phase of the G cycle, respectively.

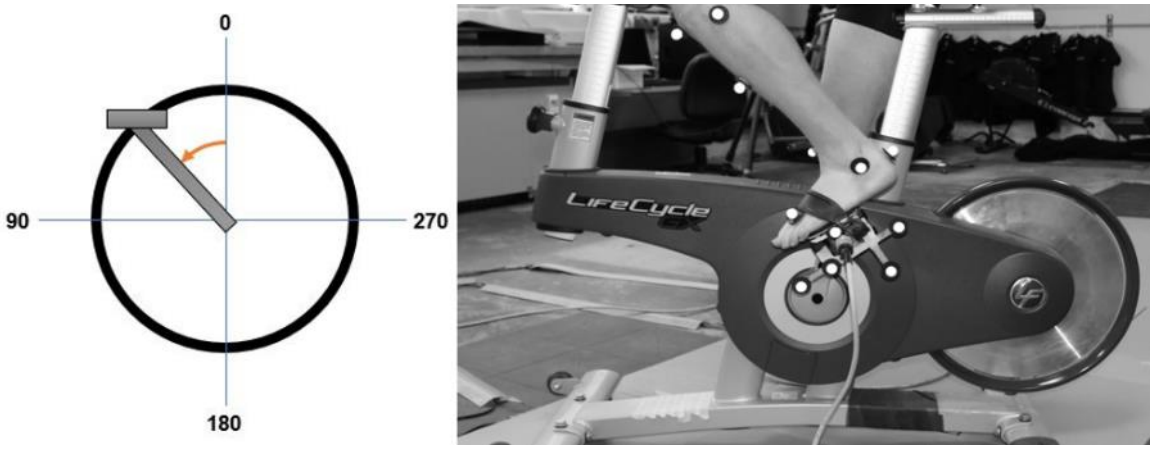

Figure 2.5: Coordinate system (left) used to define the crank angle and top dead center position for a pedal of the stationary bike.

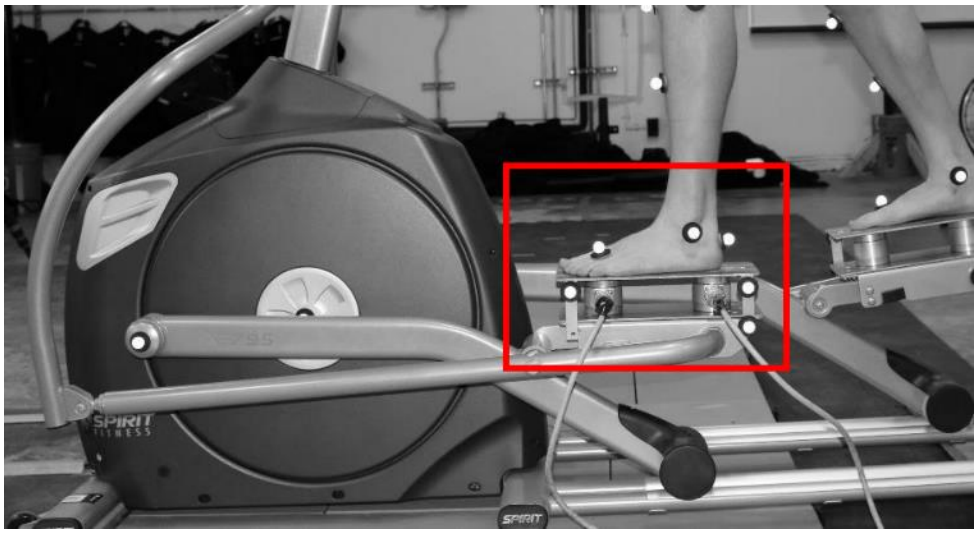

Figure 2.6: The location used to define the zero-cycle position for a pedal of the elliptical.

The dominant leg of each participant was studied. Knee angle data from the static pose of each participant was averaged, and subsequently subtracted from each participant's interpolated dynamic trials to perform a static pose offset as done in previous studies [18]. The subtraction method produced nearly identical results as multiplicative decomposition, thus the subtraction method was used to perform the static pose offset for each participant.

PCA Analysis

To implement PCA, custom code was developed in MATLAB to follow previously determined procedures [1, 2, 55, 56]. PCA was implemented to reduce crosstalk by conducting a coordinate system transformation of the calculated knee angles to minimize FE-AA correlations (Figure 2.7) [55]. From the experiment, a *nx3* matrix [***X***] of the original knee angles was collected. The means of each knee angle were subtracted from [***X***] to create a *nx3* matrix [$\boldsymbol{X_{centered}}$]. A covariance matrix [***S***] of the knee angle data was calculated as

$$[\boldsymbol{S}] = \frac{\mathbf{1}}{\boldsymbol{n-1}}[\boldsymbol{X_{centered}}]^{\boldsymbol{T}}[\boldsymbol{X_{centered}}] \quad (1)$$

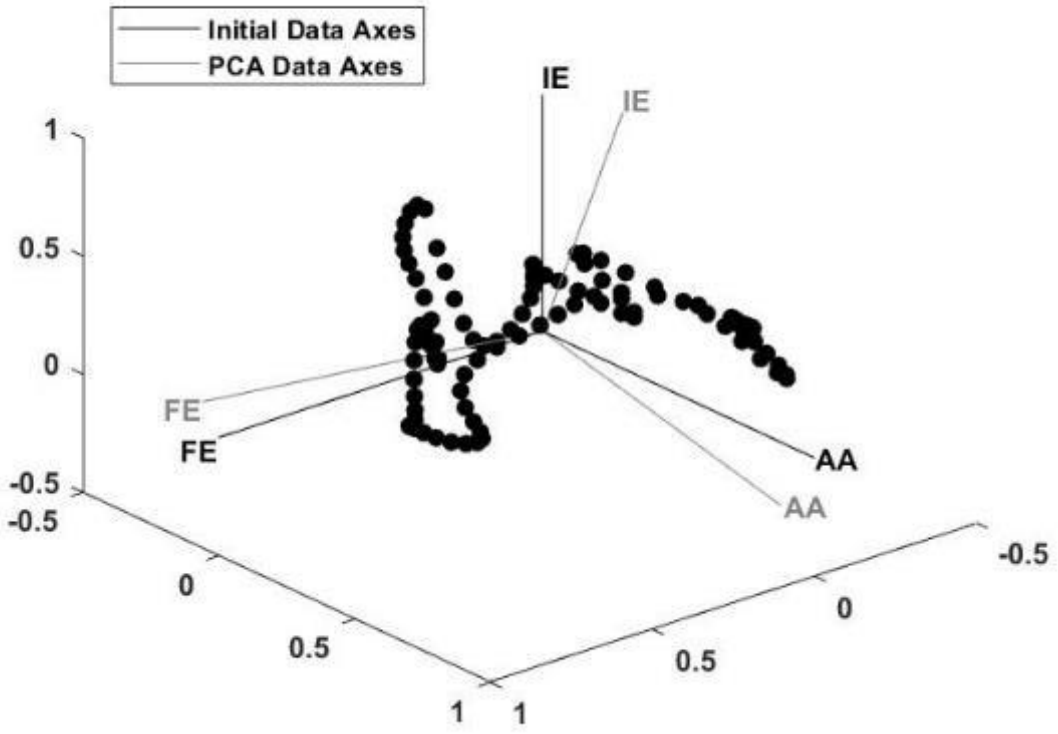

Figure 2.7: Coordinate system transformation of the data axes performed by PCA. These data axes do not represent rotation axes defined by PCA. Vectors shown are unit vectors.

An eigendecomposition of matrix [***S***] was calculated to produce a matrix of column eigenvectors, [***P***], according to

$$[\boldsymbol{S}] = [\boldsymbol{P}]^{\boldsymbol{T}}[\boldsymbol{X}][\boldsymbol{P}]. \quad (2)$$

Finally, the original knee angles, [***X***], were projected onto a new set of axes, as described by the eigenvectors in matrix [***P***]. This resulted in the calculation of a *nx3* matrix [***Z***] which contained PCA corrected FE, IR, and AA angles

$$[\boldsymbol{Z}] = [\boldsymbol{X}][\boldsymbol{P}]. \quad (3)$$

After PCA correction, the knee angles are averaged across the three trials for each subject to be used for the rest of the analysis. The correlation coefficient (R) and coefficient of determination (R^2) between the FE and AA angles were used to quantify crosstalk between the Cortex angles,

without PCA correction, and the PCA corrected angles. Larger R and R^2 values indicated the presence of greater crosstalk.

Calculating PCA Corrected Knee Axes

Previous studies that performed PCA to correct G data didn't calculate the corrected axes [1, 2]. Thus, custom MATLAB code was developed to determine the axes from the PCA corrected angles. Using Cortex and PCA corrected kinematics from dynamic trials, Cortex and simulated body vectors were calculated and PCA corrected knee axes were optimized to minimize the angle between the Cortex and simulated body vectors. The Rodrigues' rotation matrix [57] defined with a vector of rotation, $\vec{\omega}$, and angle of rotation, θ, was used to rotate vectors in 3D space by one degree-of-freedom at a time during the analysis

$$\mathbf{R}_{FE/AA/IE} = \mathbf{I} + \vec{\boldsymbol{\omega}}_{FE/AA/IE} \sin \boldsymbol{\theta}_{FE/AA/IE} + \vec{\boldsymbol{\omega}}^{\mathbf{2}}{}_{FE/AA/IE}(\mathbf{1} - \cos \boldsymbol{\theta}_{FE/AA/IE}). \quad (4)$$

Cortex knee axes were defined from marker locations during the participant's static pose. Initial body vectors were defined from the virtual joint centers calculated during the participant's static pose. Initial body segment vectors were defined with the thigh body segment aligned with [0, 0, 1], [x, y, z], to establish a local coordinate system between the Cortex and simulated body vectors. Dynamic Cortex body vectors were defined by rotating the initial body vectors about the three Cortex knee axis by each axis' corresponding angle of rotation for each of the 101 time points during the motion cycle. Cortex knee angles with static offset were used as the angles of rotation. During this process, the AA and IE axes were rotated accordingly to model joint axes motion.

Simulated body vectors were defined by rotating the initial body vectors about the FE, AA, and IE axis and the corresponding angle of rotation for each of the 101 time points during the motion cycle

$$\overrightarrow{\boldsymbol{Simulated\ Shank}}_{FE/AA/IE} = \boldsymbol{R}(\boldsymbol{\theta}_{FE/AA/IE})\, \overrightarrow{\boldsymbol{Initial\ Shank}}_{FE/AA/IE}. \quad (5)$$

The knee axes were selected by the solver and the PCA corrected knee angles with static offset were used as the angles of rotation for the determination of the rotation matrix. During the rotation of the simulated body vectors, the IE axis was rotated accordingly to follow the shank body vector

and the FE axis stayed fixed since it is defined relative to the femur [32]. After each rotation of the IE axis, a floating axis knee CS (Figure 2.8) was used [32] to redefine the AA axis using the cross product

$$\overrightarrow{\boldsymbol{AA}} = \overrightarrow{\boldsymbol{IE}} \times \overrightarrow{\boldsymbol{FE}}. \quad (6)$$

The order of rotation used was FE, AA, then IE but is not limited to this order since the final body vector location is independent of the order in which component rotations occur [32].

To determine the PCA corrected knee axes, the custom code (MATLAB) was used to determine the Cortex and simulated body vectors at each time point. An initial simulated body vector was determined using the Cortex knee axes as an initial guess for the PCA corrected knee axes. The angle between the Cortex and simulated body vectors were then determined. PCA corrected knee axes were then modified to minimize the angle between the Cortex and simulated body vectors for the entire trial. The knee axes that yielded the least error throughout the entire trial were then chosen as the PCA corrected knee axes.

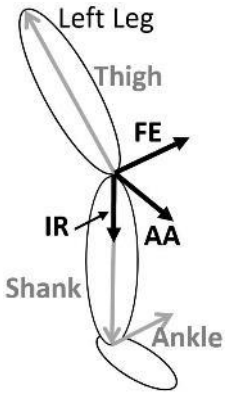

Figure 2.8: Axis (FE, IR, AA) and body (Thigh, Shank, Ankle) vectors used in analysis.

Calculating New Cycling and Elliptical Angles with Corrected Knee Axes from G

A process similar to the one described in the previous section was used to calculate new C and E angles using the PCA corrected knee axes determined from G, C and E angles from G PCA corrected axes, instead of using the knee axes defined in Cortex. In this case, the initial and dynamic Cortex body vectors were already known from previous calculations, but the initial knee axes were known instead of the angles.

The Rodrigues' rotation matrix was used again to rotate the body vectors one degree-of-freedom at a time using the axis of rotation and corresponding angle of rotation. The initial body vectors and Cortex body vectors calculated in the previous section were used again for this analysis.

To determine the simulated body vectors, the PCA corrected angles from C and E were used as initial guesses with the PCA corrected knee axes from G to rotate the initial body vectors. The error between the simulated body vectors and Cortex body vectors was calculated as the angle between the two body vectors.

The knee angles were adjusted at each time point to minimize the error between the Cortex and simulated body vectors. When the error reached the minimum value, the corresponding angles were stored. There were some stability issues when solving for the C and E knee angles with the PCA G axis which would results in spikes in the solution. The magnitude of the spikes was reduced by a custom interpolation and filtering code developed in MATLAB that used varying standard deviation values to identify data points to correct. A diagram for the non-linear solver process and for the entire analysis can be seen in Figure 2.9 and Figure 2.10, respectively.

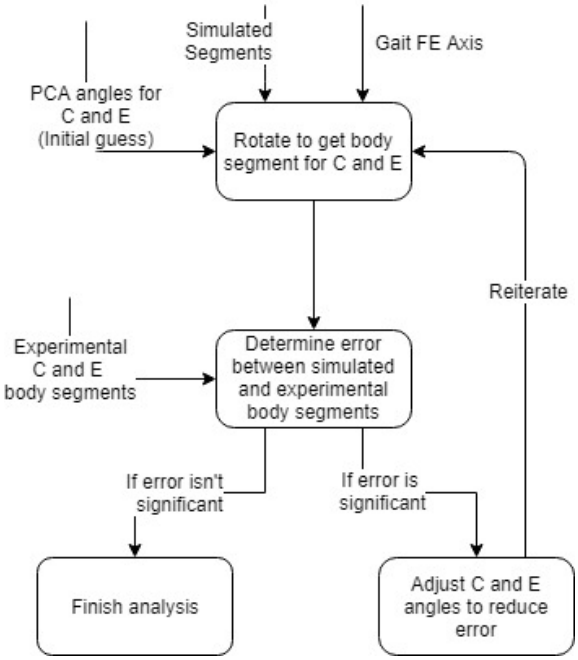

Figure 2.9: Flowchart for reprocessing the knee angles for C and E.

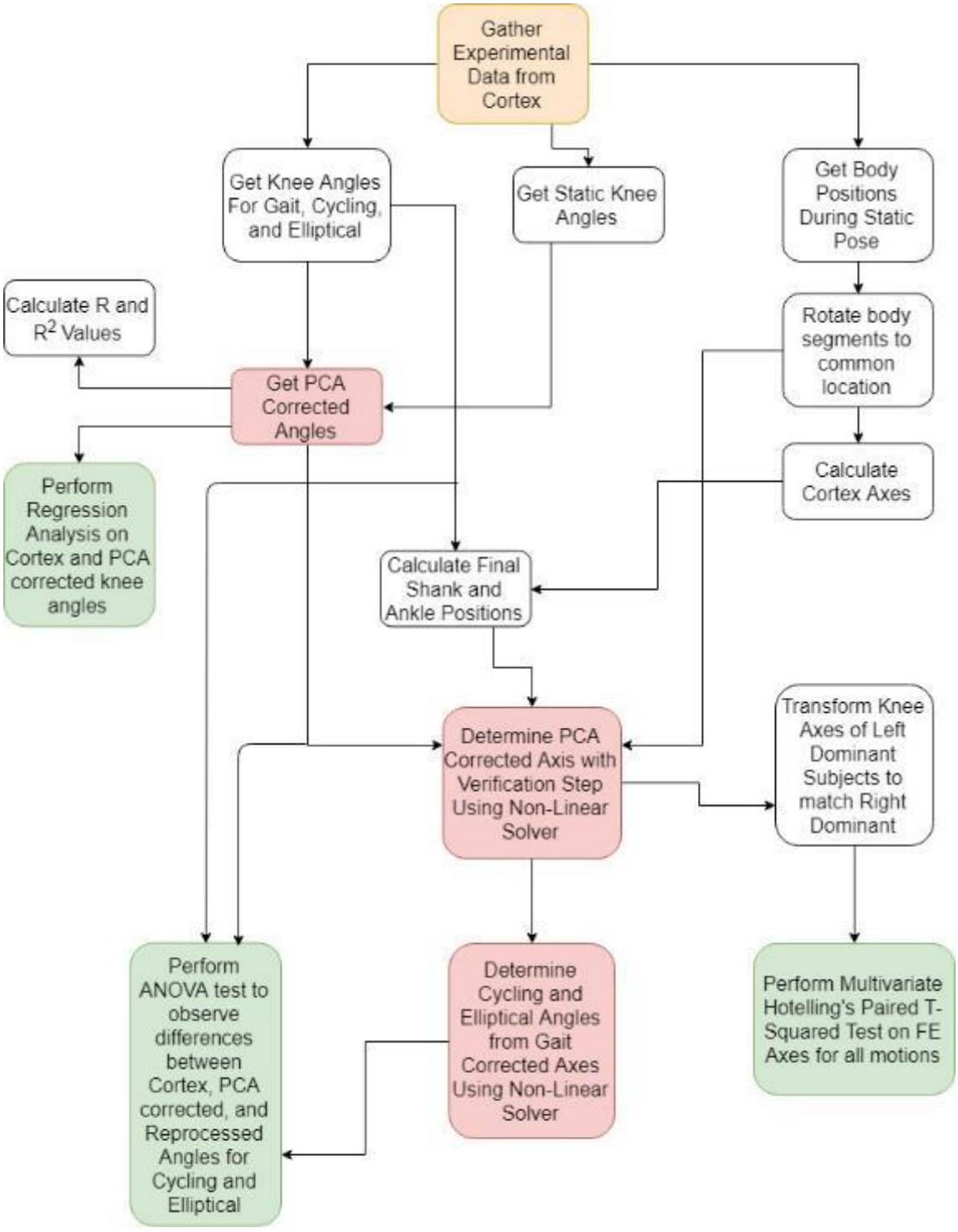

Figure 2.10: Flowchart describing the entire analysis process.

Statistics

To determine whether PCA reduced correlations between the FE and AA angles for all three exercises, regression analyses were performed on FE vs. AA angles pre- and post-PCA correction. To check for similarities between the PCA corrected G, C, and E knee axes a paired multivariate Hotelling's T-squared test was performed. In this test, the G axes was used as reference. The regression analysis and T-squared test used a significance threshold of 0.05: $p<0.05$. To check for differences in C and E angles calculated from Cortex, PCA correction, and G PCA corrected axes, an ANOVA test was performed. For the ANOVA test, the difference data line was fit with a cubic trendline following the form

$$\boldsymbol{Y = A + Bx + Cx^2 + Dx^3.} \tag{7}$$

The p-values of the coefficients were observed and if all the coefficients showed a similarity to zero then **Y** was equal to zero, thus the knee angle sets being compared were similar. If the p-values of the coefficients were observed to be different than zero, then it was concluded that the knee angle sets being compared were different. The hypothesis was rejected if a single coefficient was dissimilar to zero. Bonferroni corrections were applied to a p-value < 0.05. The 9 ANOVA tests used a significance threshold of 0.05/9: $p<0.0056$.

Chapter 3

RESULTS

Substantial crosstalk during G was found for certain participants which was expected (Figure 3.1). PCA correction resulted in negligible changes to the FE angles but noticeable changes to the AA angles (Fig 3.2-3.3). Regression analyses found reduced correlations (Table 3.1) for FE-AA angles in G ($p<0.001$ for Cortex [strongly correlated] and $p=0.851$ for PCA corrected [not correlated]), C ($p=0.011$ for Cortex and $p=0.770$ for PCA corrected), and E ($p<0.001$ for Cortex and $p=0.772$ for PCA corrected).

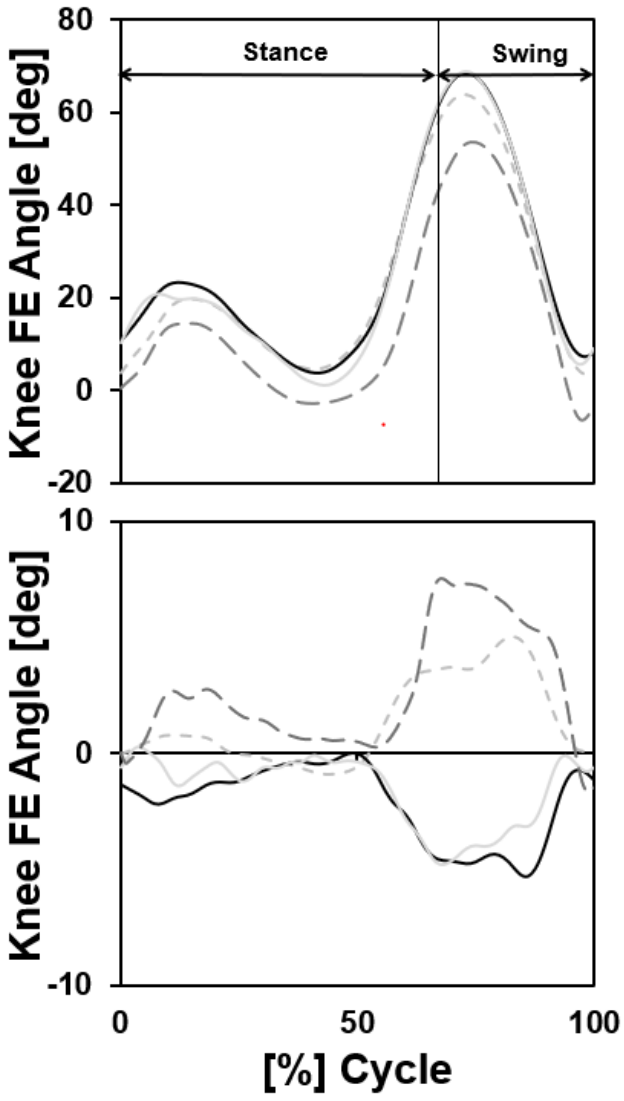

Figure 3.1: FE-AA angles from four participants with substantial crosstalk during gait (G).

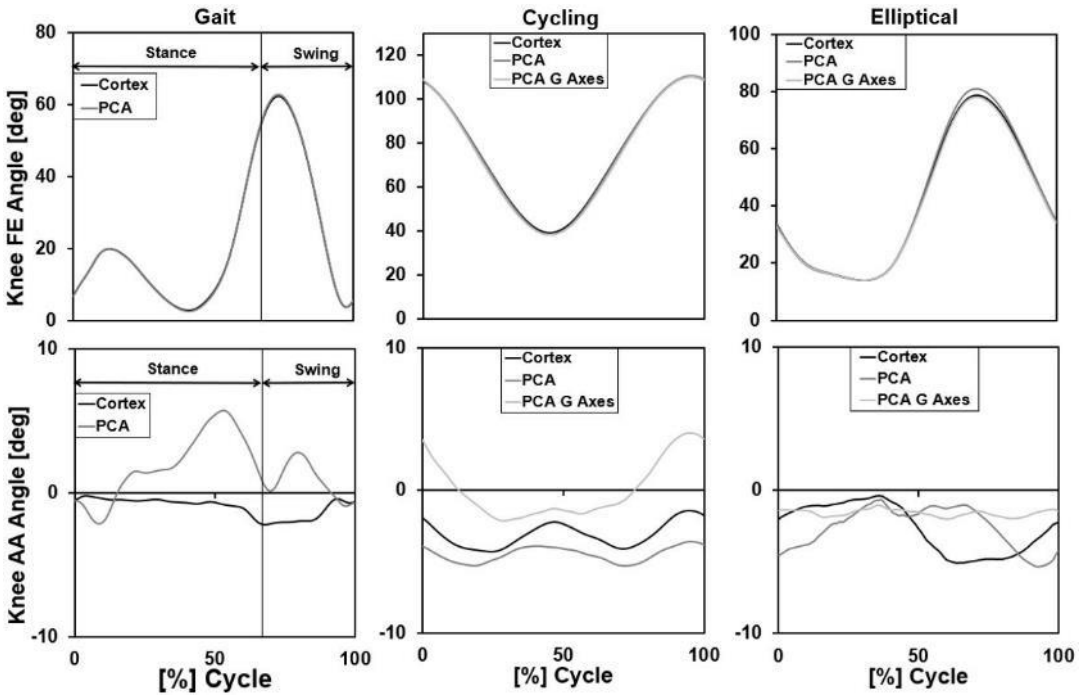

Figure 3.2: Averaged Cortex and PCA Corrected FE-AA knee angles during gait (G), cycling (C), elliptical training (E).

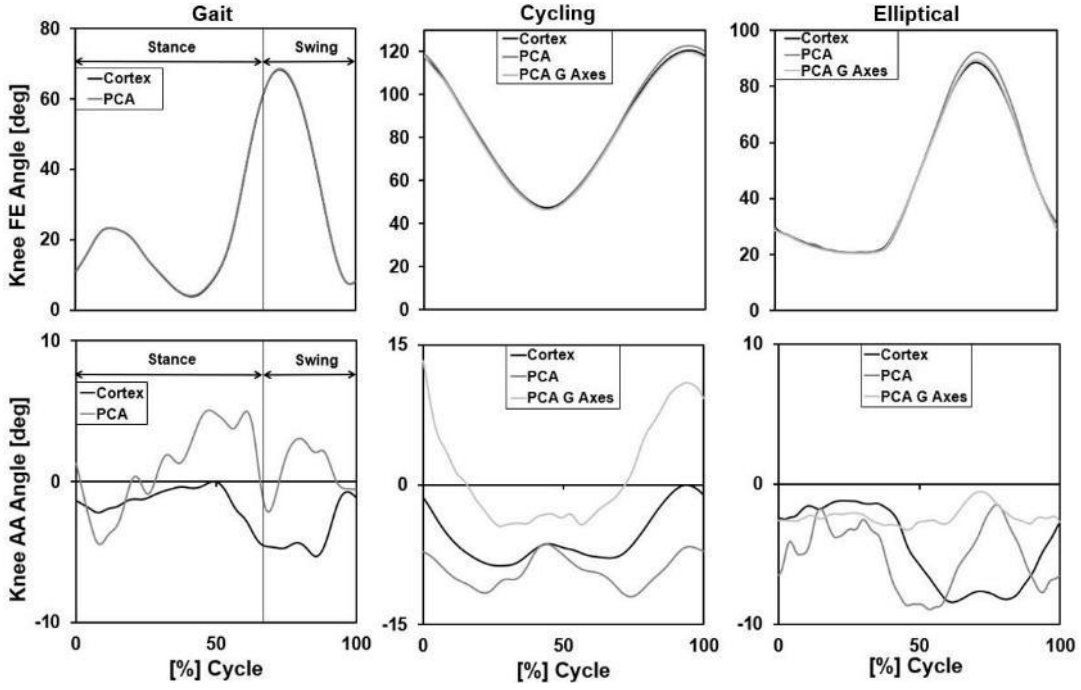

Figure 3.3: Typical FE and AA angles seen from a participant during gait (G), cycling (C), and elliptical training (E).

Table 3.1: R^2-values for FE and AA angles for pre- and post-PCA correction for gait (G), cycling (C), and elliptical training (E) exercises, and post-angle correction using G axes for C and E exercises. Mean plus/minus one standard deviation values shown. * = significant difference between cortex and PCA values.

Group	G*	C*	E*
Cortex	0.612 ± 0.287	0.415 ± 0.296	0.800 ± 0.213
PCA corrected	<0.001 ± 0.001	<0.001 ± <0.001	0.001 ± 0.002
With G PCA Axes	<0.001 ± 0.001	0.627 ± 0.297	0.446 ± 0.321

The paired multivariate Hotelling's T-squared test found significant differences in the PCA corrected knee axes between G and C and between G and E (Table 3.2, Figure 3.4).

Table 3.2: Results from Multivariate Paired Hotelling's T-Squared test for comparing the PCA corrected knee axes from cycling (C) and elliptical training (E) exercises to gait (G). * = significant difference between the PCA corrected knee axes sets.

Groups	p-value
G, C	<0.001
G, E	0.001

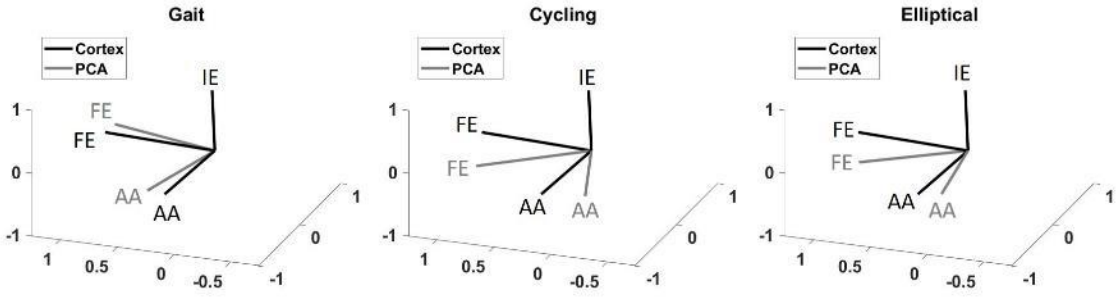

Figure 3.4: Plot showing Cortex and PCA corrected knee axes for gait (G), cycling (C), and elliptical training (E) exercises. The knee axes are represented by unit vectors.

The ANOVA test found significant differences between Cortex, PCA corrected, and the C and E knee angles when using G PCA corrected axes as most of the coefficients to the cubic trendline were significantly different than zero ($p \leq 0.002$) (Table 3.4-3.5). The AA angle differences between the three methods for a typical participant during C is shown below as a visual of Table 3.4 (Figure 3.5).

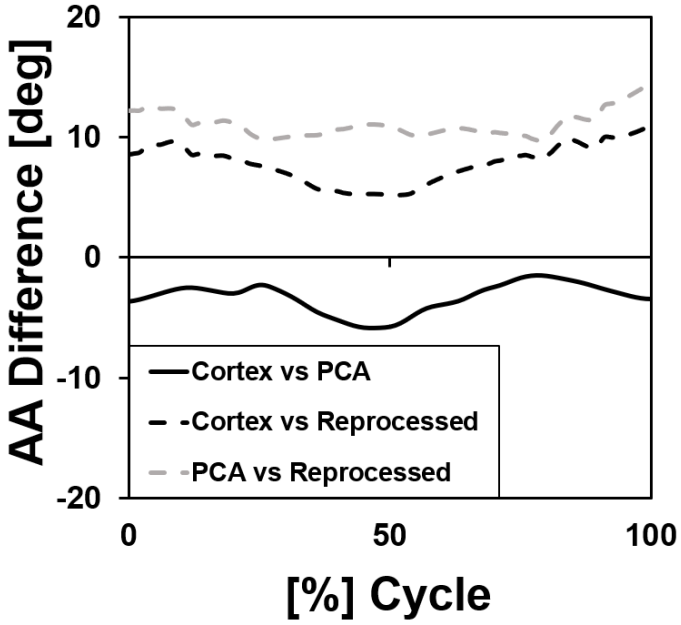

Figure 3.5: Plot showing the AA angle differences between Cortex, PCA corrected, and the knee angles when using gait (G) PCA corrected axes for a typical participant during cycling (C).

Table 3.3: ANOVA test results for comparing Cortex, PCA corrected, and PCA corrected with the G axes for cycling (C). P-values of A, B, C, and D from equation (4) are shown.

Group	Angle	A	B	C	D
Cortex	FE	<0.001	<0.001	<0.001	<0.001
vs PCA	AA	<0.001	0.001	0.004	0.043
	IE	<0.001	<0.001	<0.001	<0.001
Cortex vs	FE	0.002	<0.001	<0.001	0.005
PCA G Axes	AA	<0.001	<0.001	<0.001	<0.001
	IE	<0.001	<0.001	<0.001	<0.001
PCA vs	FE	<0.001	0.118	0.472	0.995
PCA G Axes	AA	<0.001	<0.001	<0.001	<0.001
	IE	<0.001	<0.001	<0.001	<0.001

Table 3.4: ANOVA test results for comparing Cortex, PCA corrected, and PCA corrected with the G axes for elliptical training (E). P-values of A, B, C, and D from equation (4) are shown.

Group	Angle	A	B	C	D
Cortex	FE	0.421	<0.001	<0.001	<0.001
vs PCA	AA	<0.001	<0.001	<0.001	<0.001
	IE	<0.001	<0.001	<0.001	<0.001
Cortex vs	FE	<0.001	<0.001	<0.001	<0.001
PCA G Axes	AA	<0.001	<0.001	<0.001	<0.001
	IE	<0.001	<0.001	<0.001	<0.001
PCA vs	FE	<0.001	<0.001	<0.001	<0.001
PCA G Axes	AA	<0.001	<0.001	0.012	0.363
	IE	<0.001	<0.001	<0.001	<0.001

Chapter 4

DISCUSSION

This study further demonstrated that a PCA-based algorithm can successfully reduce FE-AA correlation in all three exercises, as we hypothesized. Then, the PCA corrected knee axes differed between exercises, and for C and E, the PCA corrected knee angles were different than the knee angles calculated using G PCA corrected axes.

These results reinforce previous findings that PCA can reduce crosstalk errors in G which was also seen in other studies on crosstalk correction in G [1, 2]. However, a novel finding of the present study was the use of PCA to calculate the G PCA corrected axes. Several studies on G analysis support that there's little to no natural FE-AA correlation within the flexion angles that occur in G [50-52]. Thus, with the assumption that no FE-AA correlation exists for the flexion angle range in a G experiment, then we propose that PCA analysis of G data is an appropriate method to determine anatomical knee axes corrected for marker placement errors.

Another novel finding of the present study was that PCA can reduce FE-AA correlations in other exercises, such as C and E, that involve larger flexion angles and kinematic constraints on the feet because they remain in contact with a pedal during exercise. However, the results suggest that using PCA on C and E data may not be appropriate, because the PCA corrected axes varied between G, C, and E, and because differing FE-AA angles for C and E were calculated from PCA correction vs. when using G PCA corrected axes. These results were expected because 1) flexion angles were higher in C and E than in gait, 2) there exists evidence of natural FE-AA correlations at higher flexion angles [50-52], and 3) the foot is constrained by contact with pedals during the entire motion in C and E.

Thus, these results have important research and clinical applications when attempting to reduce crosstalk errors when considering exercise other than G. As hypothesized, corrected and subject-specific FE and AA axes produced by PCA differed for G, C, and E. Thus, PCA may not be appropriate for exercises such as C and E that involve kinematics that differ substantially from G, one option as explored in this study may be to define a common set of PCA corrected axes

from G data. Then, as done in this study, a common set of knee axes determined from G may be used without PCA correction to obtain more accurate knee angles for other exercises, such as C and E, especially those that involve relatively high flexion angles. Basically, this approach is analogous to one that would only use PCA to reduce crosstalk errors for a subset of FE-AA angles that corresponds to the relatively low flexion angles for which the assumption of no correlation between FE-AA angles would be appropriate.

This study didn't reduce the AA variability and the range in G was not as much as previous studies where markers were intentionally misplaced to create crosstalk which resulted in large AA angles pre-PCA correction [1, 2]. For one study, the lateral knee marker was intentionally placed anterior and posterior of the appropriate location and calculated pre-PCA G AA ranges of ~17 and ~23 degrees, for anterior and posterior, respectively [1]. Another study found the pre-PCA G AA range to be ~18 degrees [2]. The pre-PCA AA range found in this study for each subject was 5.42 ± 2.07 degrees which is substantially less than the range found in those two studies. Despite the differing pre-PCA G AA ranges, the PCA corrected G AA ranges were similar. In previous studies, the PCA corrected G AA ranges were ~6 and ~2 degrees [1, 2] which was found to be 9.90 ± 3.27 degrees with a minimum of 4.67 degrees for the subjects in this study. In those studies, the AA angles were only displayed for a single typical subject which makes comparison difficult.

Additional novel findings in this study were determining C and E knee angles that were similar to those found in previous studies. In general, our FE angles agreed qualitatively with previous studies for C [58] and E [59-62]. AA angle ranges higher than G were predicted for C which corroborated with a previous study for C [58] but were higher than the AA angle range found in another study [63]. Low AA angle ranges were predicted for E which matched the results from a study on kinematics during E [64] and was lower than measured in a previous study [61].

This study has a few limitations. First, our methods didn't incorporate techniques to eliminate errors induced by soft tissue artifact which is considered another leading source of error in motion analysis studies. Second, it is still unclear how to best reduce crosstalk errors when

studying G with other exercises that involve larger FE values. Regardless, a novel contribution of this study was the development and recommendation of one standardized protocol that involves using PCA only for G data, and then finding the G PCA corrected axes and using those axes to recalculate angles in C and E. Third, requiring the use of non-linear solvers to determine the PCA corrected axes, and the C and E knee angles using the G PCA corrected axes, may be a limiting factor for other gait and motion analysis labs as it requires specific software and complex algorithms. Though the algorithm was complex, it didn't yield an exact solution due to the system of equations used to find the axes and angles being over constrained from having more equations than unknowns. Thus, two solutions were calculated by the solver for the PCA corrected knee axes for each trial and the C and E angles from G PCA corrected axes for each time point. From each of the two solutions, a single solution was determined using interpolation based on the objective functions set inside the solver. The opposite case would be to have more unknowns than equations, thus making the problem indeterminate. A problem with an equal amount of equations as unknowns can be solved for an exact solution. To help mitigate this limitation, future efforts could be to publish algorithms for open-access use and development.

This study supports that PCA is an effective post hoc technique for reducing crosstalk in gait but not in cycling or elliptical training due to differing kinematics. A protocol is proposed to use PCA only for gait data, then using the G PCA corrected axes as subject-specific axes and to determine angles in activities with larger knee FE values than in G. The findings of this paper support that PCA is an effective correction technique to determine angles and axes that represent accurate knee motion and can be beneficial for motion analysis and rehabilitative surgery or consultation.

REFERENCES

[1] E. Jensen, V. Lugade, J. Crenshaw, E. Miller and K. Kaufman, "A principal component analysis approach to correcting the knee flexion axis during gait," *Journal of Biomechanics,* vol. 49, no. 9, pp. 1698-1704, 2016.

[2] A. Baudet, C. Morisset, P. d'Athis, J.-F. Maillefert, J.-M. Casillas, P. Ornetti and D. Laroche, "Cross-Talk Correction Method for Knee Kinematics in Gait Analysis Using Principal Component Analysis (PCA): A New Proposal," *PLOS One,* vol. 9, no. 7, 2014.

[3] A. Ferrari, M. G. Benedetti, E. Pavan, C. Frigo, D. Bettinelli, M. Rabuffetti, P. Crenna and A. Leardini, "Quantitative comparison of five current protocols in gait analysis," *Gait & Posture,* vol. 28, pp. 207-216, 2008.

[4] M. A. Robinson and J. Vanrenterghem, "An evaluation of anatomical and functional knee axis definition in the context of side-cutting," *Journal of Biomechanics,* vol. 45, pp. 1941-1946, 2012.

[5] M. H. Schwartz, J. P. Trost and R. A. Wervey, "Measurement and management of errors in quantitative gait data," *Gait & Posture,* vol. 20, pp. 196-203, 2004.

[6] E. Most, J. Axe, H. Rubash and G. Li, "Sensitivity of the knee joint kinematics calculation to selection of flexion axes," *Journal of Biomechanics,* vol. 37, pp. 1743-1748, 2004.

[7] M. Freeman and V. Pinskerova, "The movement of the normal tibio-femoral joint," *Journal of Biomechanics,* vol. 38, pp. 197-208, 2005.

[8] S. J. Piazza and P. R. Cavanagh, "Measurement of the screw-home motion of the knee is sensitive to errors in axis alignment," *Journal of Biomechanics,* vol. 33, pp. 1029-1034, 2000.

[9] D. K. Ramsey and P. F. Wretenberg, "Biomechanics of the knee: methodological considerations in the in vivo kinematic analysis of the tibiofemoral and patellofemoral joint," *Clinical Biomechanics,* vol. 14, pp. 595-611, 1999.

[10] R. Baker, L. Finney and J. Orr, "A new approach to determine the hip rotation profile from clinical gait analysis data," *Human Movement Science,* vol. 18, pp. 655-667, 1999.

[11] I. W. Charlton, P. Tate, P. Smyth and L. Roren, "Repeatability of an optimised lower body model," *Gait & Posture,* vol. 20, pp. 213-221, 2004.

[12] R. M. Ehrig, W. R. Taylor, G. N. Duda and M. O. Heller, "A survey of formal methods for determining functional joint axes," *Journal of Biomechanics,* vol. 40, pp. 2150-2157, 2007.

[13] A. G. Schache, R. Baker and L. W. Lamoreux, "Defining the knee joint flexion-extension axis for purposes of quantitative gait analysis: An evaluation of methods," *Gait & Posture,* vol. 24, pp. 100-109, 2006.

[14] F. Marin, H. Mannel, L. Claes and L. Durselen, "Correction of axis misalignment in the analysis of knee rotations," *Human Movement Science,* vol. 22, pp. 285-296, 2003.

[15] B. E. Groen, M. Geurts, B. Nienhuis and J. Duysens, "Sensitivity of the OLGA and VCM models to erroneous marker placement: Effects on 3D-gait kinematics," *Gait & Posture,* vol. 35, pp. 517-521, 2012.

[16] L.-P. Rivest, "A correction for axis misalignment in the joint angle curves representing knee movement in gait analysis," *Journal of Biomechanics,* vol. 38, pp. 1604-1611, 2005.

[17] H. J. Woltring, "3-D attitude representation of human joints: a standardization proposal," *Journal of Biomechanics,* vol. 27, no. 12, pp. 1399-1414, 1994.

[18] A. Leardini, Z. Sawacha, G. Paolini, S. Ingrosso, R. Nativo and M. G. Benedetti, "A new anatomically based protocol for gait analysis in children," *Gait & Posture,* vol. 26, no. 4, pp. 560-571, 2007.

[19] M. C. d. M. Filho, R. Yoshida, W. d. S. Carvalho, H. E. Stein and N. F. Novo, "Are the recommendations from three-dimensional gait analysis associated with better posoperative outcomes in patients with cerebral palsy?," *Gait & Posture,* no. 28, pp. 316-322, 2008.

[20] B. Lofterod and T. Terjesen, "Results of treatment when orthopaedic surgeons follow gait-analysis recommendations in children with CP," *Development Medicine & Child Neurology,* no. 50, pp. 503-509, 2008.

[21] V. Saraph, E.-B. Zwick, G. Zwick, C. Steinwender, G. Steinwender and W. Linhart, "Multilevel Surgery in Spastic Diplegia: Evaluation by Physical Examination and Gait Analysis in 25 Children," *Journal of Pediatric Orthopedics,* vol. 22, pp. 150-157, 2002.

[22] T. A. Wren, N. Y. Otsuka, R. E. Bowen, A. A. Scaduto, L. S. Chan, M. Sheng, R. Hara and R. M. Kay, "Influence of gait analysis on decision-making for lower extremeity orthopaedic surgery: Baseline data from randomized controlled trial," *Gait & Posture,* no. 34, pp. 364-369, 2011.

[23] A. Aminian, S. J. Vankoski, L. Dias and R. A. Novak, "Spastic Hemiplegic Cerebral Palsy and the Fermoral Derotation Osteotomy: Effect at the Pelvis and Hip in the Transverse Plane During Gait," *Journal of Pediatric Orthopaedics,* vol. 23, pp. 314-320, 2003.

[24] P. A. DeLuca, R. B. Davis III, S. Ounpuu, S. Rose and R. Sirkin, "Alterations in Surgical Decision Making in Patients with Cerebral Palsy Based on Three-Dimensional Gait Analysis," *Journal of Pediatric Orthopaedics,* vol. 17, pp. 608-614, 1997.

[25] K. J. Bell, S. Ounpuu, P. A. DeLuca and M. J. Romness, "Natural Progression of Gait in Children With Cerebral Palsy," *Journal of Pediatric Orthopaedics,* vol. 22, pp. 677-682, 2002.

[26] J. T. Bennett, W. P. Bunnell and G. D. MacEwen, "Rotational Osteotomy of the Distal Tibia and Fibula," *Journal of Pediatric Orthopaedics,* vol. 5, pp. 294-298, 1985.

[27] R. M. Stefko, R. J. de Swart, D. Dodgin, M. P. Wyatt, K. R. Kaufmann, D. H. Sutherland and H. G. Chambers, "Kinematic and Kinetic Analysis of Distal Derotational Osteotomy of the Leg in Children with Cerebral Palsy," *Journal of Pediatric Orthopaedics,* vol. 18, pp. 81-87, 1998.

[28] W. F. Krengel and L. T. Staheli, "Tibial Rotational Osteotomy for Idiopathic Torsion," *Clinical Orthopaedics and Related Research,* no. 283, pp. 285-289, 1992.

[29] L. T. Staheli, M. Corbett, C. Wyss and H. King, "Lower-Extremity Rotational Problems in Children," *The Journal of Bone and Joint Surgery,* vol. 67, pp. 39-47, 1985.

[30] K. A. Ball and T. M. Greiner, "On the problems of describing joint axis alignment," *Journal of Biomechanics,* vol. 41, pp. 1599-1603, 2008.

[31] H. K. Ramakrishnan and M. P. Kadaba, "On The Estimation of Joint Kinematics During Gait," *Journal of Biomechanics,* vol. 24, no. 10, pp. 969-977, 1991.

[32] E. S. Grood and W. J. Suntay, "A Joint Coordinate System for the Clinical Description of Three-Dimensional Motions: Application to the Knee," *Journal of Biomechanical Engineering,* vol. 105, pp. 136-144, 1983.

[33] A. Cappozzo, F. Catani, U. Della Croce and A. Leardini, "Position and orientation in space of bones during movement: anatomical frame definition and determination," *Clinical Biomechanics,* vol. 10, no. 4, pp. 171-178, 1995.

[34] U. Della Croce, A. Cappozzo and D. C. Kerrigan, "Pelvis and lower limb anatomical landmark calibration precision and its propagation to bone geometry and joint angles," *Medical & Biological Engineering & Computing,* vol. 37, pp. 155-161, 1999.

[35] M. Donati, V. Camomilla, G. Vannozzi and A. Cappozzo, "Enhanced anatomical calibration in human movement analysis," *Gait & Posture,* vol. 26, pp. 179-185, 2007.

[36] G. Wu and P. R. Cavanagh, "ISB recommendations for standardization in the reporting of kinematic data," *Journal of Biomechanics,* vol. 28, no. 10, pp. 1257-1261, 1995.

[37] S. J. Tupling and M. R. Pierrynowski, "Use of cardan angles to locate rigid bodies in three-dimensional space," *Medical & biological engineering & computing,* vol. 25, no. 5, pp. 527-532, 1987.

[38] E. Szczerbik and M. Kalinowska, "The influence of knee marker placement error on evaluation of gait kinematics parameters," *Acta of Bioengineering and Biomechanics,* vol. 13, no. 3, pp. 43-46, 2011.

[39] G. E. Gorton III, D. A. Herbert and M. E. Gannotti, "Assessment of the kinematic variability among 12 motion analysis laboratories," *Gait & Posture,* vol. 29, pp. 398-402, 2009.

[40] M. P. Kadaba, H. K. Ramakrishnan, M. E. Wootten, J. Gainey, G. Gorton and G. V. B. Cochran, "Repeatability of Kinematic, Kinetic, and Electromyographic Data in Normal Adult Gait," *Journal of Orthopaedic Research,* vol. 7, pp. 849-860, 1989.

[41] M. P. Kadaba, H. K. Ramakrishnan and M. E. Wootten, "Measurement of Lower Extremity Kinematics During Level Walking," *Journal of Orthopaedic Research,* vol. 8, pp. 383-392, 1990.

[42] L. Cheze, "Comparison of different calculations of three-dimensional joint kinematics from video-based system data," *Journal of Biomechanics,* vol. 33, pp. 1695-1699, 2000.

[43] L. Blankevoort, R. Huiskes and A. De Lange, "The Envelope of Passive Knee Joint Motion," *Journal of Biomechanics,* vol. 21, no. 9, pp. 705-720, 1988.

[44] M. A. Lafortune, P. R. Cavanagh, H. J. Sommer III and A. Kalenak, "Three-Dimensional Kinematics of The Human Knee During Walking," *Journal of Biomechanics,* vol. 25, no. 4, pp. 347-357, 1992.

[45] C. Reinschmidt, A. J. van den Bogert, B. M. Nigg, A. Lundberg and N. Murphy, "Effect of skin movement on the analysis of skeletal knee joint motion during running," *Journal of Biomechanics,* vol. 30, no. 7, pp. 729-732, 1997.

[46] M. H. Schwartz and A. Rozumalski, "A new method for estimating joint parameters from motion data," *Journal of Biomechanics,* vol. 38, pp. 107-116, 2005.

[47] K. Halvorsen, M. Lesser and A. Lundberg, "A new method for estimating the axis of rotation and the center of rotation," *Journal of Biomechanics,* vol. 32, pp. 1221-1227, 1999.

[48] J. Lasenby and S. S. H. U. Gamage, "New least squares solutions for estimating the average centre of rotation and the axis of rotation," *Journal of Biomechanics,* vol. 35, pp. 87-93, 2002.

[49] A. M. Fullenkamp, J. G. Richards and D. J. Hudson, "DYNAMIC KNEE AXIS ALIGNMENT: A CLINICAL COMPARISON".

[50] B. Yu, M. J. Stuart, E. S. Growney and K.-N. An, "Valgus-varus motion of the knee in normal level walking and stair climbing," *Clinical Biomechanics,* vol. 12, no. 5, pp. 286-293, 1997.

[51] D. R. Wilson, J. D. Feikes, A. B. Zavatsky and J. J. O'Connor, "The components of passive knee movement are coupled to flexion angle," *Journal of Biomechanics,* vol. 33, pp. 465-473, 2000.

[52] E. S. Grood, S. F. Stowers and F. R. Noyes, "Limits of Movement in the Human Knee," *The Journal of Bone and Joint Surgery,* vol. 70, pp. 88-97, 1988.

[53] Centers for Disease Control and Prevention, "About Adult BMI," 29 August 2017. [Online]. Available: https://www.cdc.gov/healthyweight/assessing/bmi/adult_bmi/index.html. [Accessed 10 March 2018].

[54] J. D. Gutierrez-Franco, "THE EFFECTS OF OBESITY ON RESULTANT KNEE JOINT LOADS FOR GAIT AND CYCLING," California Polytechnic State University San Luis Obispo, San Luis Obispo, 2016.

[55] J. Shlens, "A TUTORIAL ON PRINCIPAL COMPONENT ANALYSIS," arXiv, 2003.

[56] I. T. Jolliffe, in *Principal component analysis*, Springer-Verlang, 1986, p. 296.

[57] M. D. Shuster, "A Survey of Attitude Representations," *The Journal of the Astronautical Sciences,* vol. 41, no. 4, pp. 429-517, 1993.

[58] M. P. Bailey, F. J. Maillardet and N. Messenger, "Kinematics of cycling in relation to anterior knee pain and patellar tendinitis," *Journal of Sports Science,* vol. 21, pp. 649-657, 2003.

[59] J. M. Burnfield, Y. Shu, T. Buster and A. Taylor, "Similarity of Joint Kinematics and Muscle Demands Between Elliptical Training and Walking: Implications for Practice," *Physical Therapy,* vol. 90, no. 2, pp. 289-305, 2010.

[60] K. M. Knutzen, W. L. McLaughlin, A. J. Lawson, B. S. Row and L. T. Martin, "Influence of Ramp Position on Joint Biomechanics During Elliptical Trainer Exercise," *The Open Sports Science Journal,* vol. 3, pp. 165-177, 2010.

[61] T.-W. Lu, H.-L. Chien and H.-L. Chen, "Joint Loading in the Lower Extremities during Elliptical Exercise," *Medicine & Science in Sports & Exercise,* vol. 39, no. 9, pp. 1651-1658, 2007.

[62] M. J. Rogatzki, T. W. Kernozek, J. D. Willson, J. F. Greany, D.-A. Hong and J. P. Porcari, "Peak Muscle Activation, Joint Kinematics, and Kinetics During Elliptical and Stepping Movement Pattern on a Precor Adaptive Motion Trainer," *Research Quarterly for Exercise and Sport,* vol. 83, no. 2, pp. 152-159, 2012.

[63] T. F. Boyd, R. R. Neptune and M. L. Hull, "Pedal and knee loads using a multi-degree-of-freedom pedal platform in cycling," *Journal of Biomechanics,* vol. 30, no. 5, pp. 505-511, 1997.

[64] M. R. Paquette, A. Zucker-Levin, P. DeVita, J. Hoekstra and D. Pearsall, "Lower Limb Joint Angular Position and Muscle Activity During Elliptical Exercise in Healthy Young Men," *Journal of Applied Biomechanics,* vol. 31, pp. 19-27, 2015.

Appendix A: FE-AA plots for all subjects

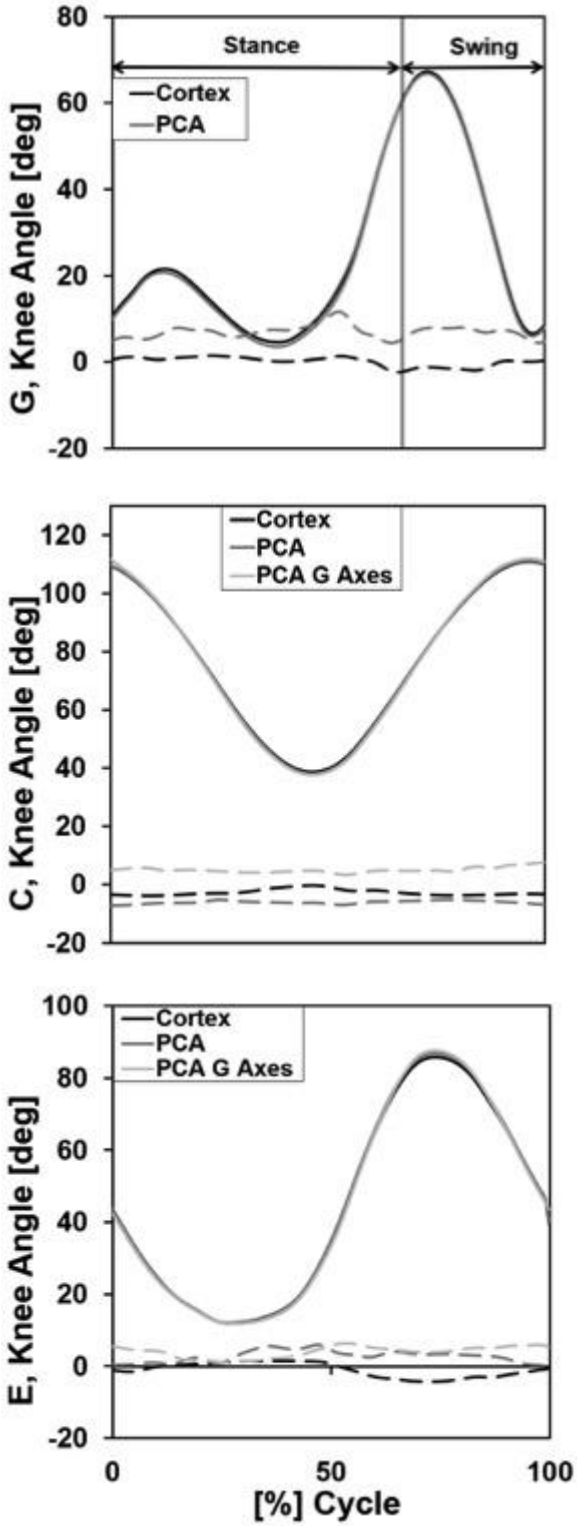

Figure A-1: FE-AA angles for subject 2016Aug12-02 during gait (G), cycling (C), and elliptical training (E).

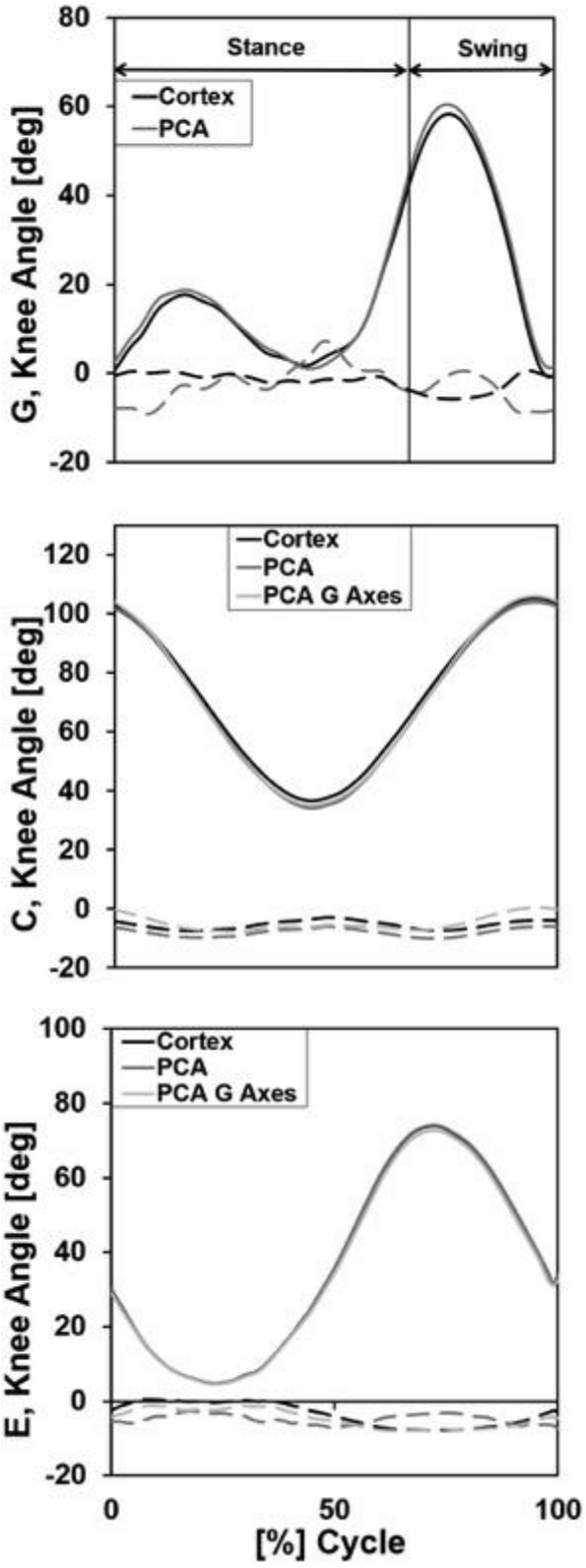

Figure A-2: FE-AA angles for subject 2016Aug15-01 during gait (G), cycling (C), and elliptical training (E).

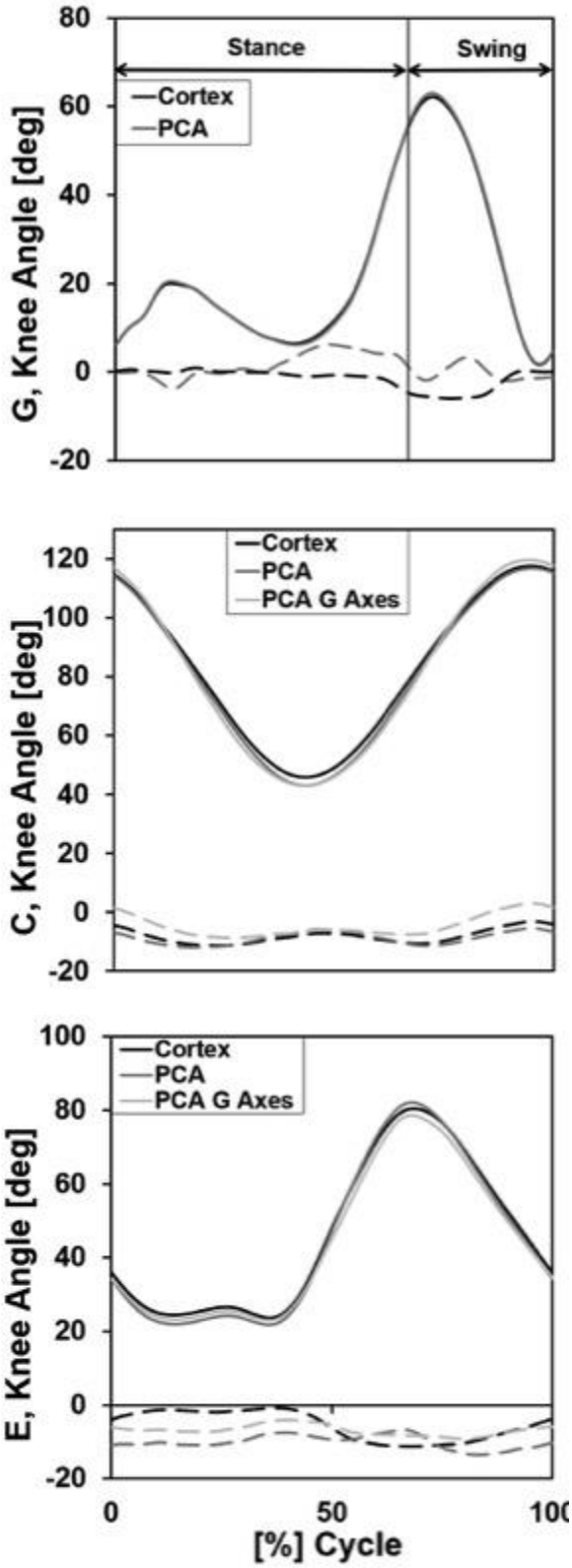

Figure A-3: FE-AA angles for subject 2016Aug19-01 during gait (G), cycling (C), and elliptical training (E).

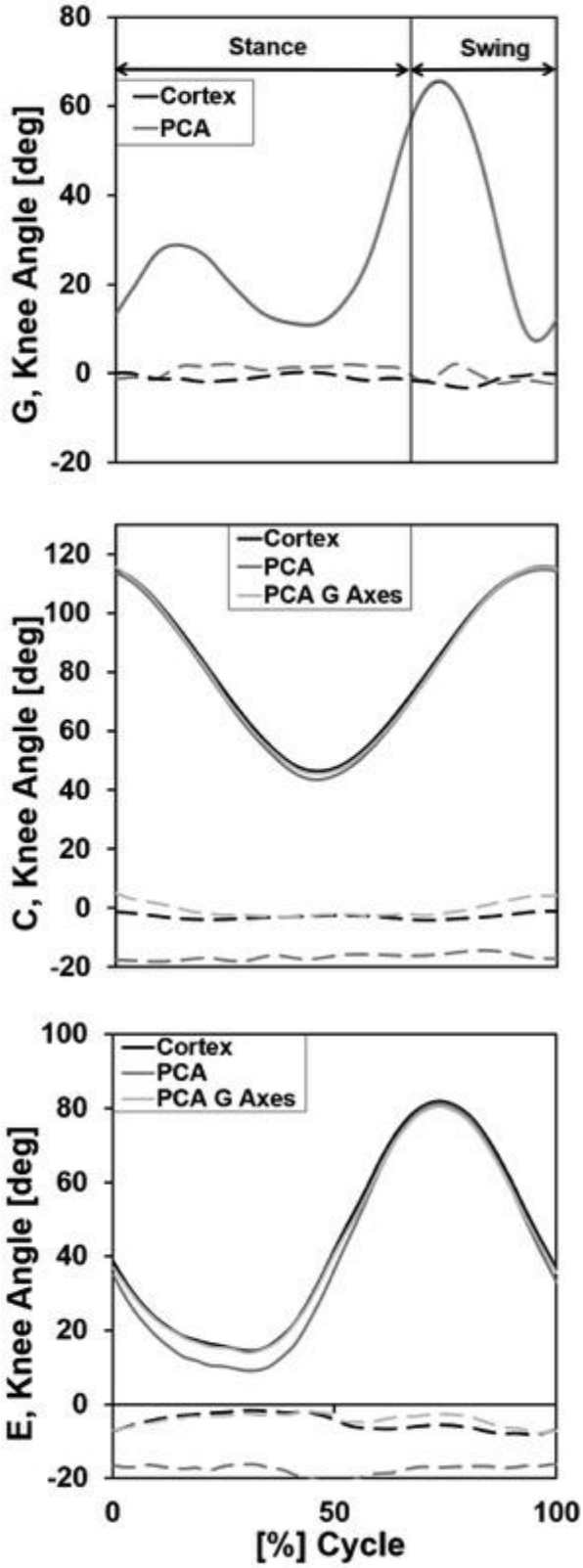

Figure A-4: FE-AA angles for subject 2016Aug26-01 during gait (G), cycling (C), and elliptical training (E).

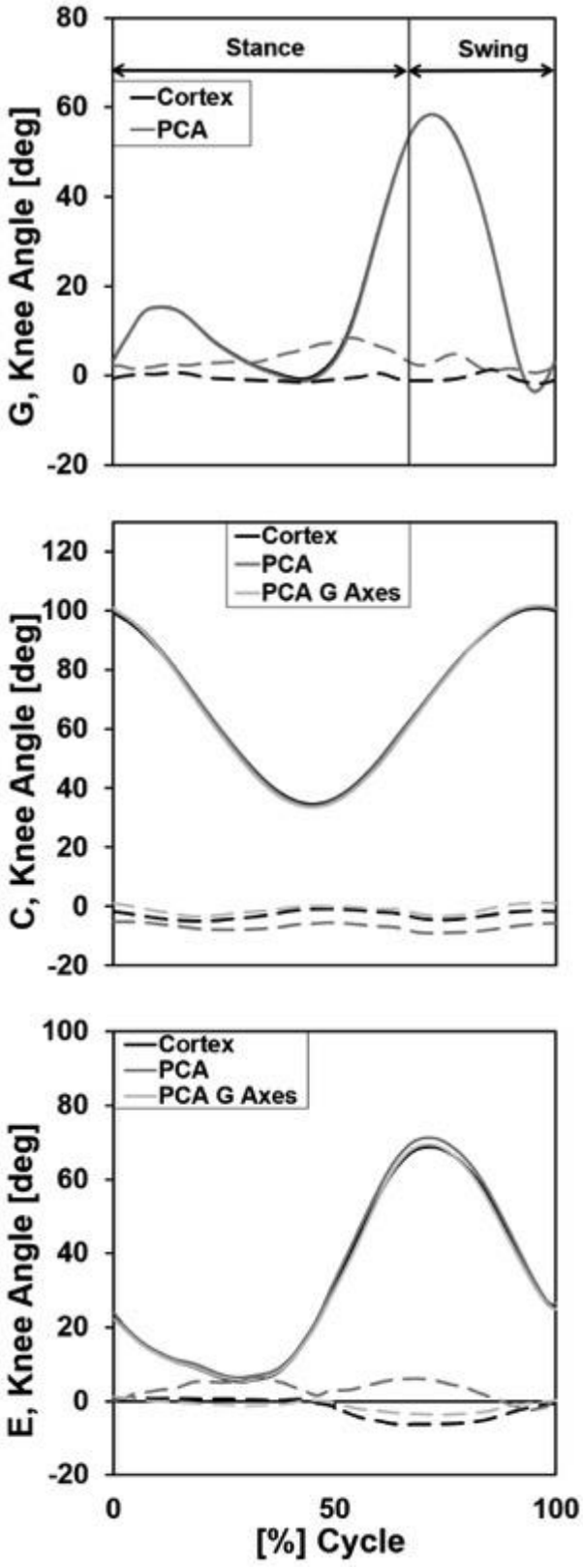

Figure A-5: FE-AA angles for subject 2016Sep01-01 during gait (G), cycling (C), and elliptical training (E).

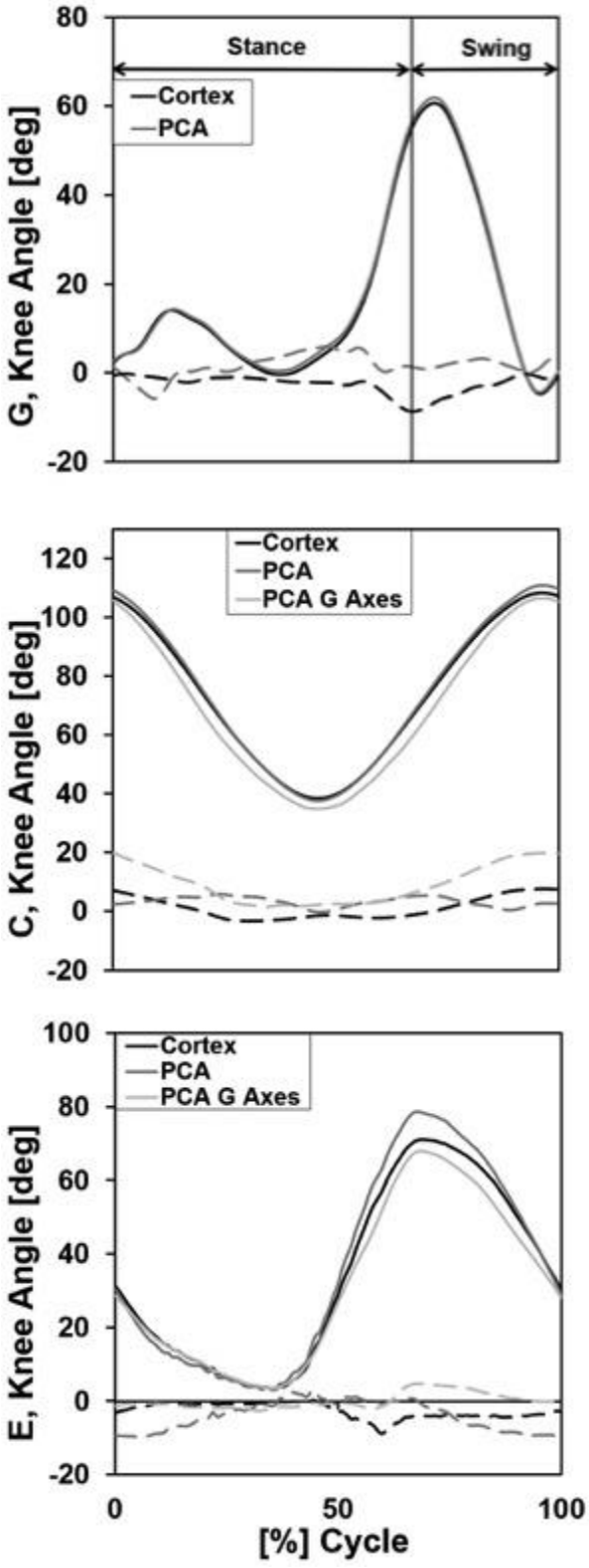

Figure A-6: FE-AA angles for subject 2016Nov05-01 during gait (G), cycling (C), and elliptical training (E).

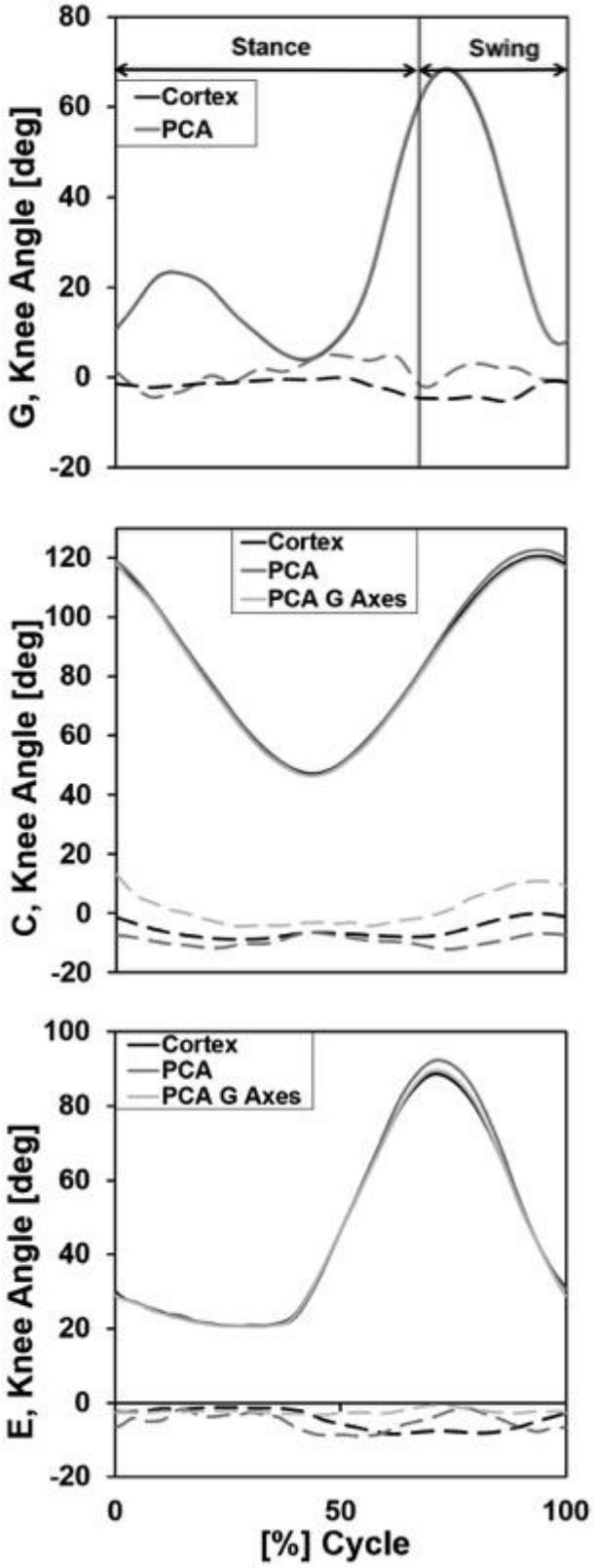

Figure A-7: FE-AA angles for subject 2017Jun19-01 during gait (G), cycling (C), and elliptical training (E).

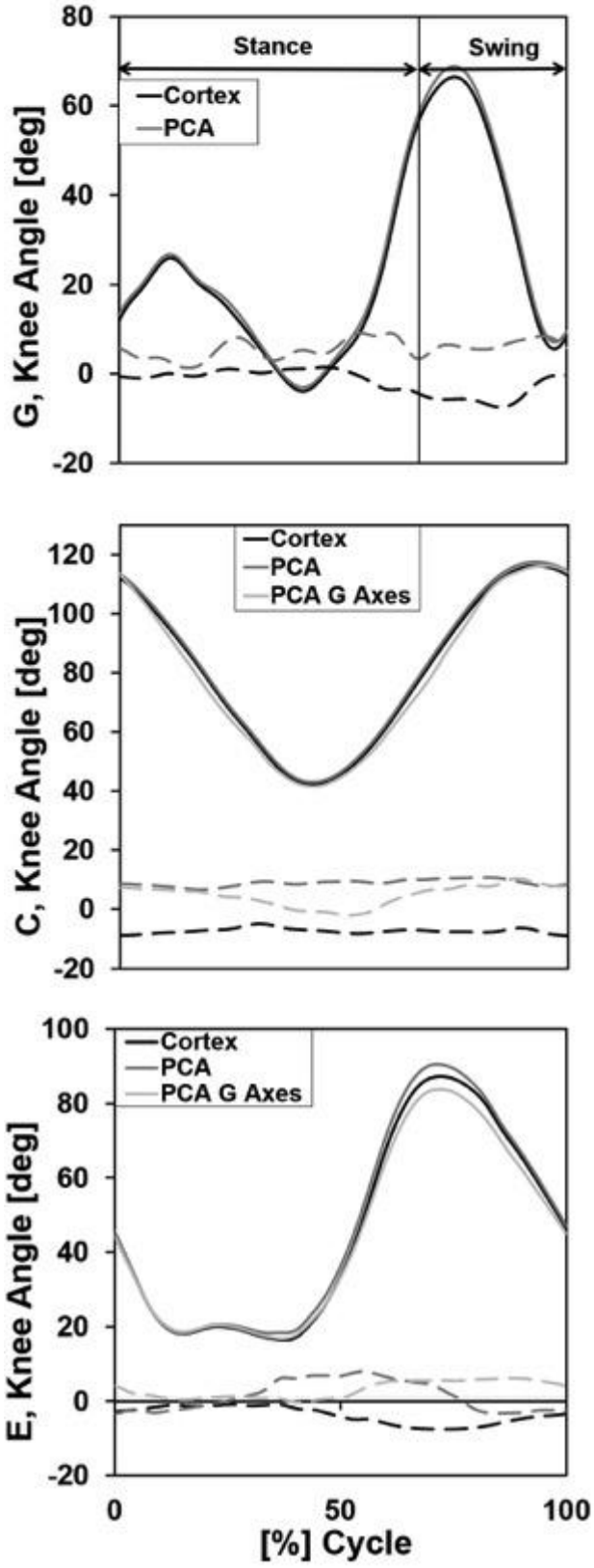

Figure A-8: FE-AA angles for subject 2017Jun19-02 during gait (G), cycling (C), and elliptical training (E).

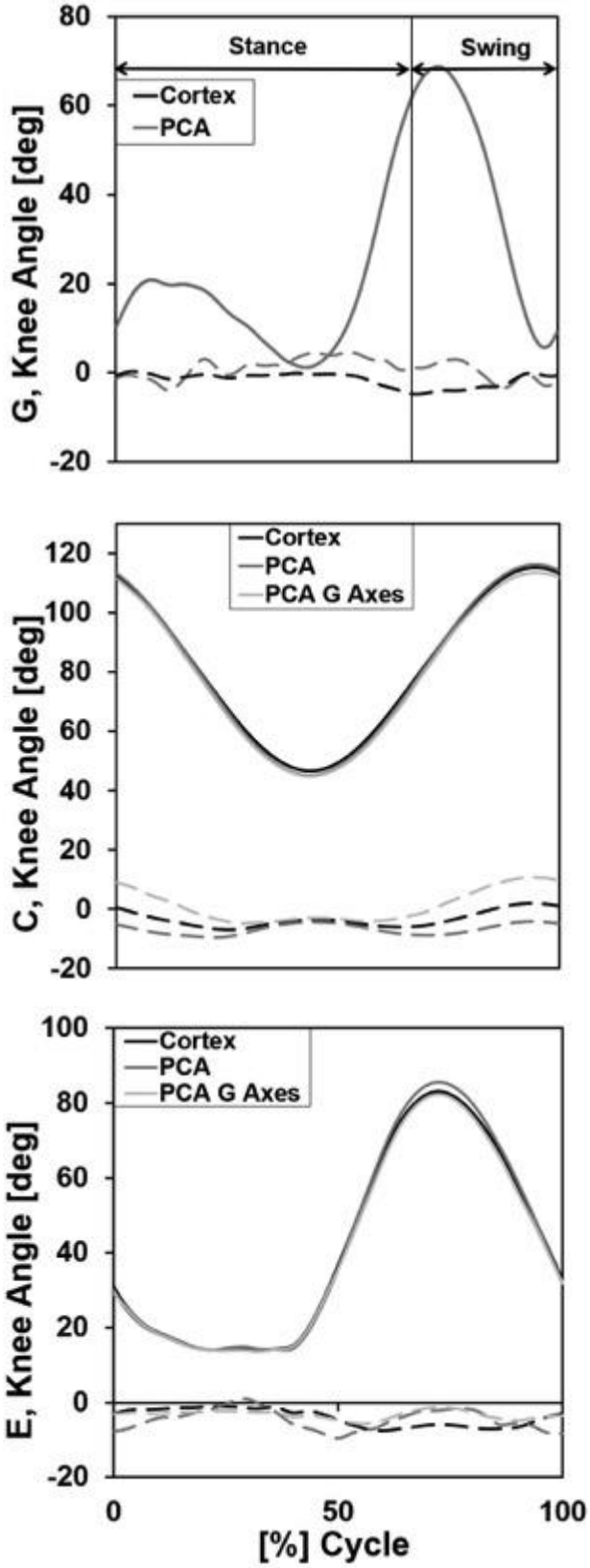

Figure A-9: FE-AA angles for subject 2017Jun27-01 during gait (G), cycling (C), and elliptical training (E).

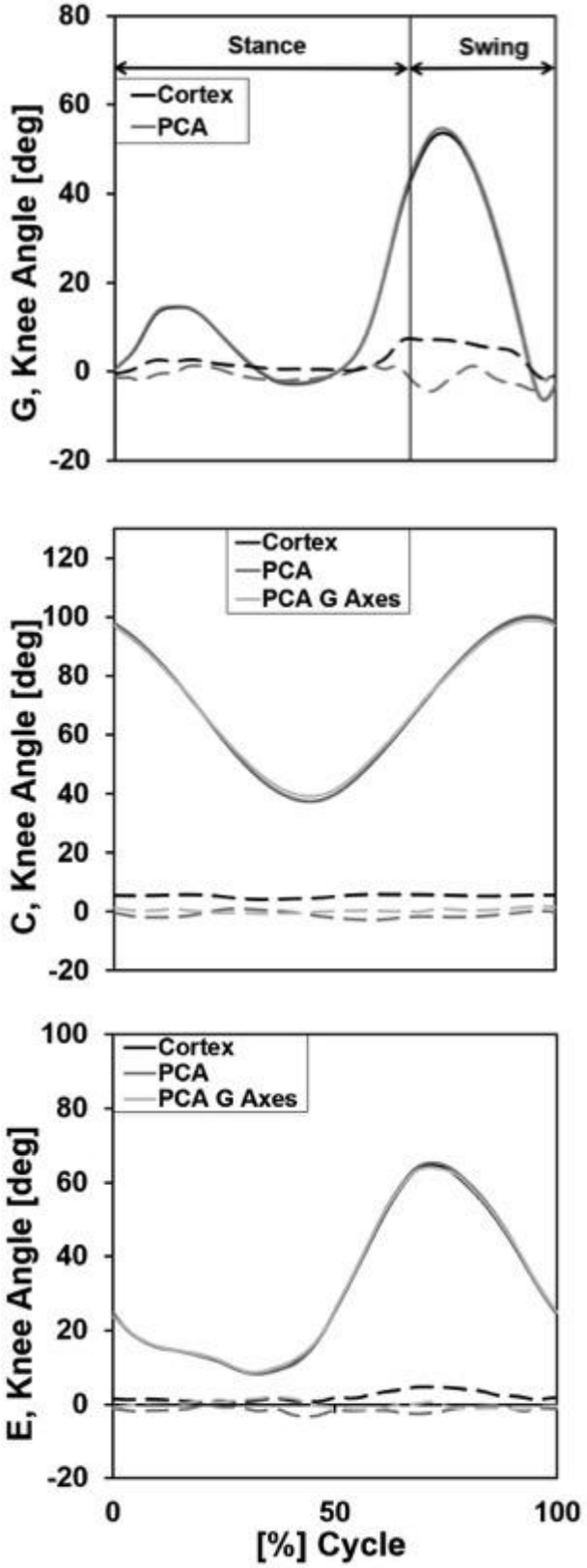

Figure A-10: FE-AA angles for subject 2017Jul20-01 during gait (G), cycling (C), and elliptical training (E).

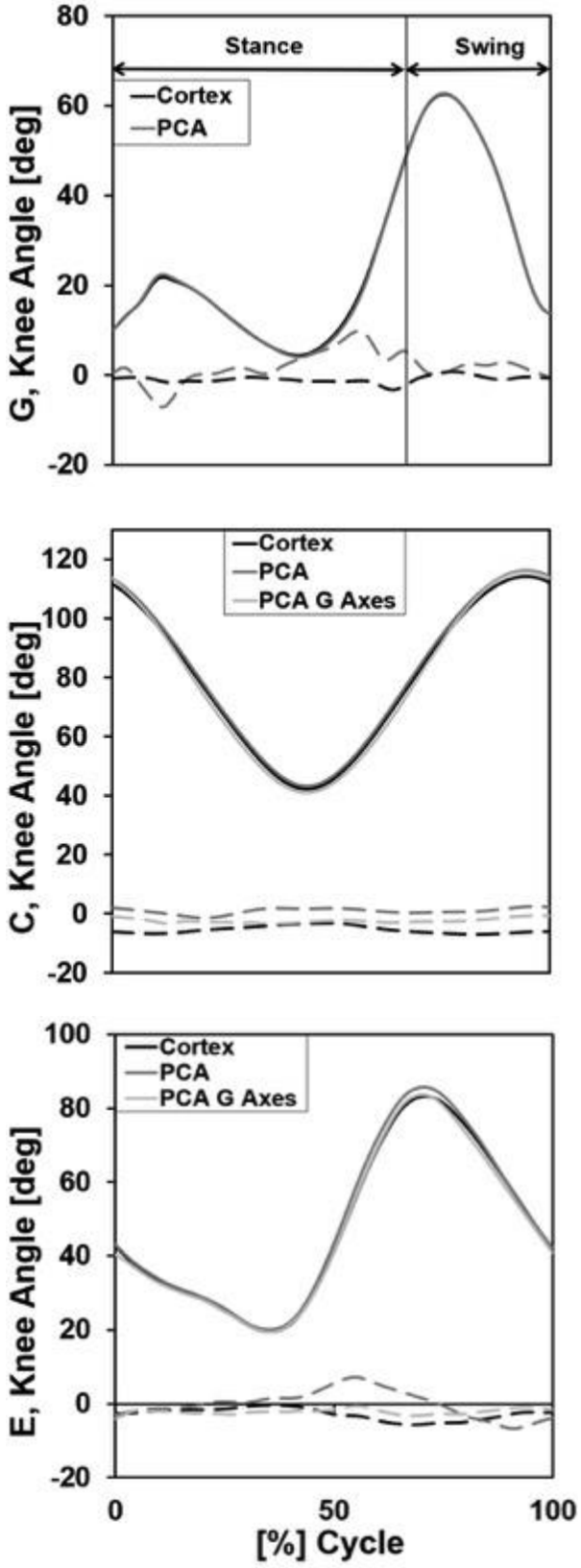

Figure A-11: FE-AA angles for subject 2017Jul20-02 during gait (G), cycling (C), and elliptical training (E).

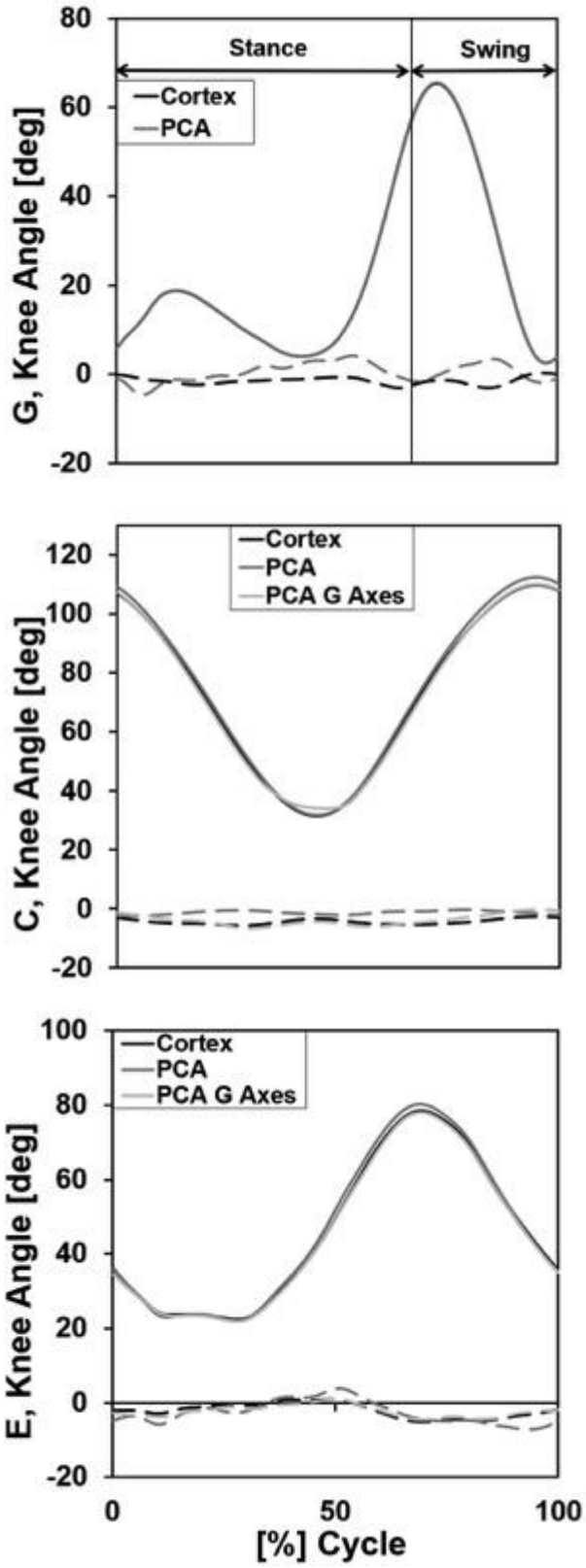

Figure A-12: FE-AA angles for subject 2017Jul24-01 during gait (G), cycling (C), and elliptical training (E).

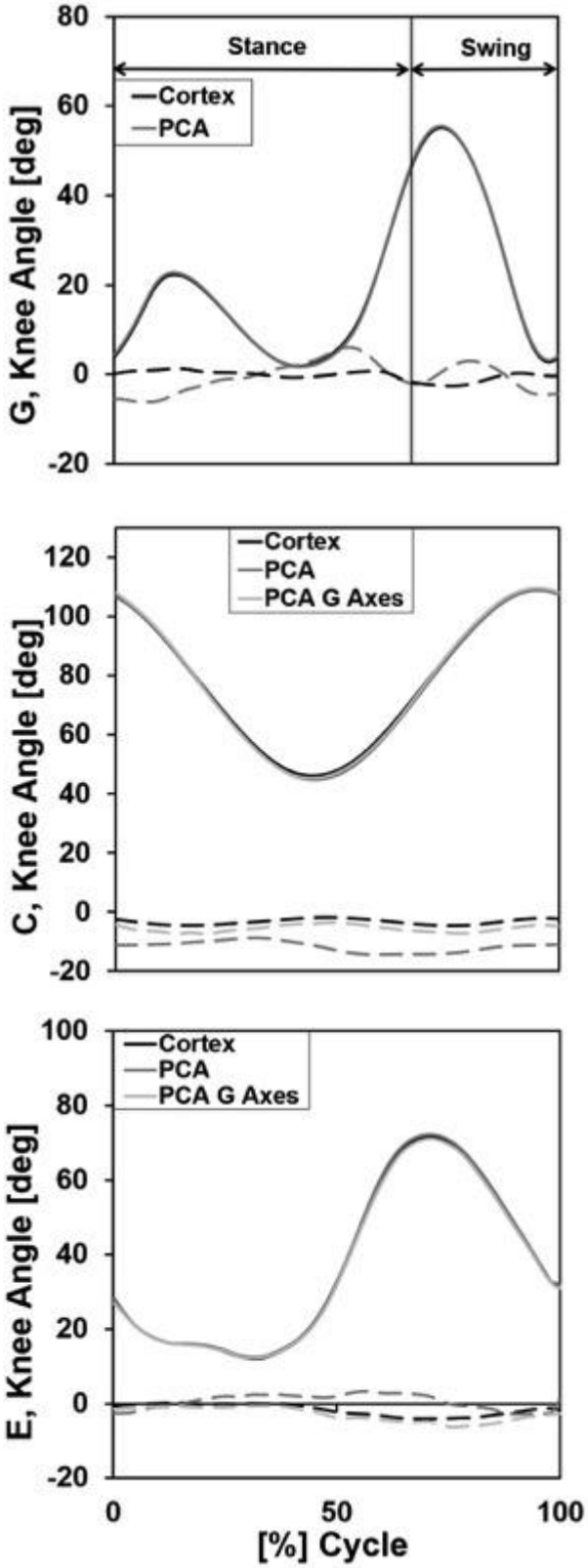

Figure A-13: FE-AA angles for subject 2018Jan22-01 during gait (G), cycling (C), and elliptical training (E).

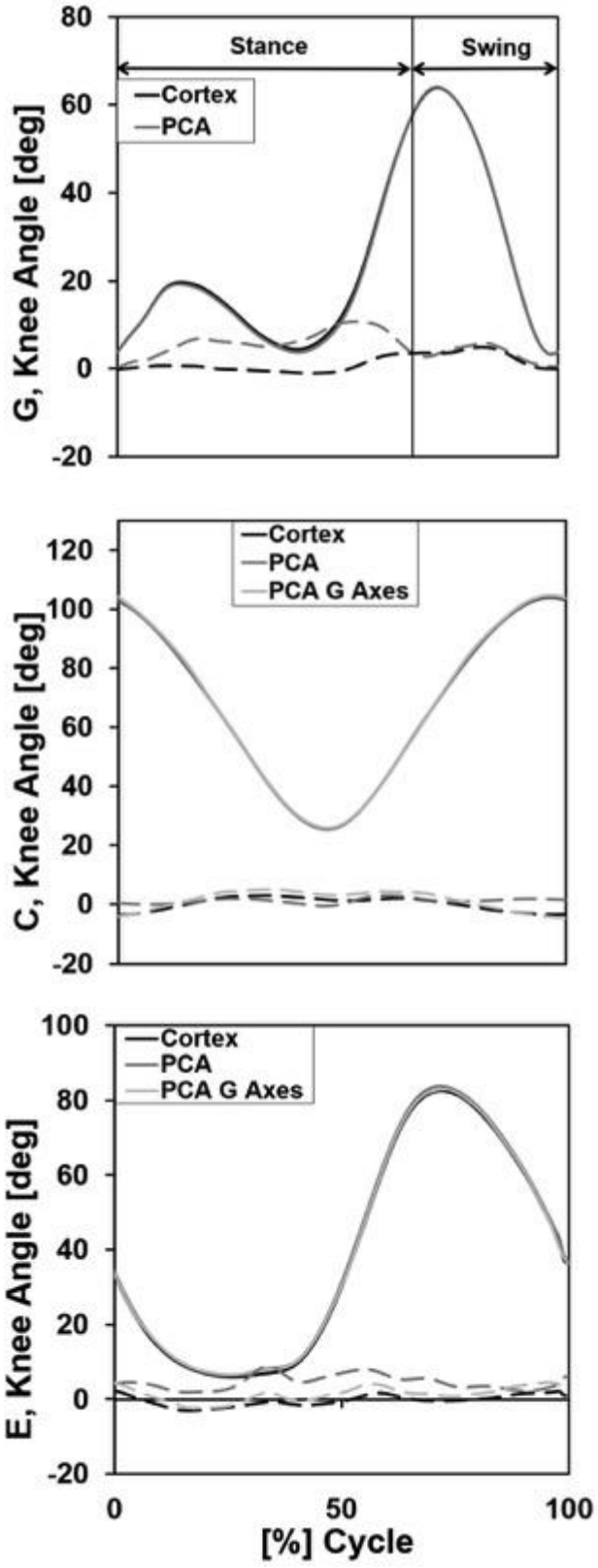

Figure A-14: FE-AA angles for subject 2018Feb15-01 during gait (G), cycling (C), and elliptical training (E).

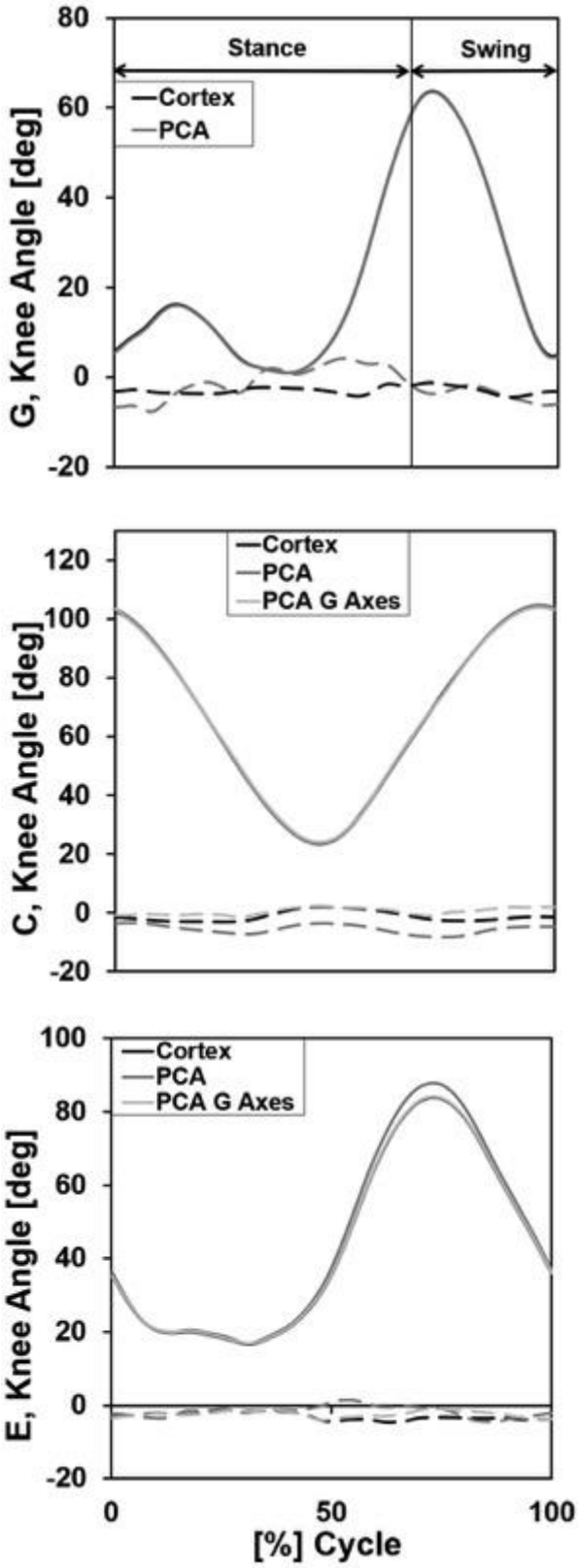

Figure A-15: FE-AA angles for subject 2018Feb15-02 during gait (G), cycling (C), and elliptical training (E).

Appendix B: Principal Component Analysis (PCA)

In this appendix, a detailed explanation on how to perform a data transformation using PCA will be given. PCA functions by minimizing the covariance between the variables in the data set of interest. With the original knee angle data organized into a *nx3* matrix, [**X**], which contains the three knee angles FE, AA, and IR at *n* distinct time points. The data set, [**X**], is then "re-centered" by subtracting each column's mean from itself to produce [$\mathbf{X}_{\mathbf{centered}}$]. The covariance matrix, [**S**], of [$\mathbf{X}_{\mathbf{centered}}$] is calculated using equation (1). An eigendecomposition of matrix [**S**] is calculated to produce a matrix of column eigenvectors, [**P**], according to equation (2). The final step is to project the original knee angles, [**X**], onto a new set of axes, as described by the eigenvectors in matrix [**P**], to define the data space which eliminate correlation between the knee angles. This produces a *nx3* matrix [***Z***] which contains PCA corrected FE, AA, and IR angles at n distinct time points using equation (3).

Appendix C: Multiplicative Decomposition

In this study, the subtraction method was compared to multiplicative decomposition by comparing the rotation matrices corresponding to the relative angles from the dynamic and static angles using both methods. The subtraction method defines the relative angles as the dynamic angles minus the static angles. Multiplicative decomposition is used when performing configuration transformations for bodies in three-dimensional space.

Body segments were rotated from an initial configuration to the final configuration with the use of static, relative, and dynamic configuration transformations as shown by:

$$\overrightarrow{\boldsymbol{V}_{\boldsymbol{final}}} = [Dynamic]\,\overrightarrow{\boldsymbol{V}_{\boldsymbol{initial}}} = [Relative]\,[Static]\,\overrightarrow{\boldsymbol{V}_{\boldsymbol{initial}}} \quad (8)$$

To show how the Rodrigues' rotation matrix is used which each of the three independent joint rotations the relationship between the dynamic, relative, and static configurations can be written as:

$$[[FE][AA][IR]]_{dynamic}\,\overrightarrow{\boldsymbol{V}_{\boldsymbol{initial}}} = [[FE][AA][IR]]_{relative}\,[[FE][AA][IR]]_{static}\,\overrightarrow{\boldsymbol{V}_{\boldsymbol{initial}}} \quad (9)$$

Each of the FE, AA, and IR rotation matrices are determined using the Rodrigues' rotation matrix with the respective knee angles and axis. The static and dynamic configurations can be determined using the knee angles during the static trial and G, C, and E trials, respectively, and the knee axis corresponding to the angle. With the matrices corresponding to the static and dynamic configurations known, the relative configuration can be calculated as such:

$$[Relative] = [Dynamic][Static]^{-1} \quad (10)$$

With the matrix corresponding to the relative configuration known, the joint angles corresponding to the dynamic position relative to the subject's anatomical posture could be determined. To determine the relative joint angles, a non-linear solver was used to find the FE, AA, and IR angles that created a 3x3 matrix equal to that determined in equation 5 when used with the Rodrigues' rotation matrix and the subject's joint axes.

These relative angles were then compared to those determined using the subtraction method used in another study [1] and determined to have a negligible difference. Thus, the subtraction method was used.

Appendix D: Multiplicative Decomposition vs "Subtraction" Method Calculations

Table D-1: All randomly generated test cases with their corresponding static and dynamic knee angles and the shank error magnitude.

	Static Angles (deg.)			Dynamic Angles (deg.)			
Case	FE	AA	IE	FE	AA	IE	Shank Error Magnitude
1	12.58	-0.60	-26.92	99.26	2.48	-11.52	0.0000
2	0.52	7.07	0.15	110.46	-12.97	-14.80	0.0040
3	6.62	3.14	-20.54	14.68	7.30	7.21	0.0005
4	11.32	2.57	-11.23	111.40	9.42	8.92	0.0007
5	15.98	8.45	-26.77	76.83	3.06	-25.96	0.0002
6	11.06	5.03	-8.60	17.64	5.03	-8.60	0.0001
7	7.62	5.89	-22.60	33.31	4.66	-11.13	0.0004
8	-2.31	5.83	-5.86	66.32	-4.08	0.38	0.0003
9	-2.05	-0.14	-4.35	116.83	2.48	3.99	0.0000
10	0.58	2.86	-1.83	117.73	-9.59	6.59	0.0008
11	14.76	-5.02	-14.57	18.44	3.74	-20.85	0.0002
12	0.50	-5.37	-30.28	118.43	-13.06	2.29	0.0031
13	14.12	2.26	24.06	116.78	-6.95	0.88	0.0003
14	0.24	6.24	5.24	58.76	-12.70	-27.35	0.0034
15	16.91	8.72	-27.34	97.49	-11.43	-29.85	0.0036
16	2.83	-4.15	1.50	16.51	6.66	-8.10	0.0006
17	-0.90	2.87	-10.81	50.93	3.46	18.35	0.0001
18	0.42	1.28	8.79	111.69	-5.95	-17.16	0.0001
19	9.30	-6.04	-30.52	96.49	9.82	-3.12	0.0018
20	5.83	-0.84	-14.91	117.07	-13.00	-23.84	0.0005

Table D-2: The rotation matrices calculated using the two multiplicative decomposition combinations and using the standard method for cases 1-10.

Case	Rotation matrix following [Dynamic]*[Static]$^{-1}$	Rotation matrix following [Static]$^{-1}$*[Dynamic]	Rotation matrix following the standard method
1	$\begin{bmatrix} 0.042 & -0.067 & 0.997 \\ 0.265 & 0.963 & 0.054 \\ 0.963 & 0.262 & 0.058 \end{bmatrix}$	$\begin{bmatrix} 0.042 & -0.067 & 0.997 \\ 0.265 & 0.963 & 0.054 \\ 0.963 & 0.262 & 0.058 \end{bmatrix}$	$\begin{bmatrix} 0.042 & 0.067 & 0.997 \\ 0.265 & 0.963 & 0.054 \\ 0.963 & 0.262 & 0.058 \end{bmatrix}$
2	$\begin{bmatrix} -0.412 & 0.222 & 0.883 \\ -0.242 & 0.908 & -0.341 \\ -0.878 & -0.355 & -0.320 \end{bmatrix}$	$\begin{bmatrix} 0.412 & 0.220 & 0.884 \\ -0.242 & 0.908 & -0.340 \\ -0.878 & -0.354 & -0.321 \end{bmatrix}$	$\begin{bmatrix} -0.413 & 0.223 & 0.883 \\ -0.242 & 0.908 & -0.343 \\ -0.878 & -0.355 & -0.320 \end{bmatrix}$
3	$\begin{bmatrix} 0.871 & -0.470 & 0.140 \\ 0.464 & 0.883 & 0.072 \\ -0.157 & 0.002 & 0.987 \end{bmatrix}$	$\begin{bmatrix} 0.871 & -0.470 & 0.140 \\ 0.464 & 0.883 & 0.073 \\ -0.157 & 0.002 & 0.987 \end{bmatrix}$	$\begin{bmatrix} 0.871 & -0.470 & 0.140 \\ 0.464 & 0.883 & 0.073 \\ -0.157 & 0.002 & 0.987 \end{bmatrix}$
4	$\begin{bmatrix} -0.205 & -0.050 & 0.977 \\ 0.342 & 0.932 & 0.119 \\ -0.917 & 0.359 & -0.174 \end{bmatrix}$	$\begin{bmatrix} -0.205 & -0.050 & 0.977 \\ 0.342 & 0.932 & 0.120 \\ -0.917 & 0.359 & -0.174 \end{bmatrix}$	$\begin{bmatrix} -0.205 & -0.050 & 0.977 \\ 0.342 & 0.932 & 0.119 \\ -0.917 & 0.359 & -0.174 \end{bmatrix}$
5	$\begin{bmatrix} 0.488 & 0.076 & 0.869 \\ 0.014 & 0.995 & -0.095 \\ -0.873 & 0.058 & 0.485 \end{bmatrix}$	$\begin{bmatrix} 0.488 & 0.075 & 0.869 \\ 0.014 & 0.995 & -0.095 \\ -0.873 & 0.058 & 0.485 \end{bmatrix}$	$\begin{bmatrix} 0.488 & 0.075 & 0.869 \\ 0.014 & 0.995 & -0.094 \\ -0.873 & 0.058 & 0.485 \end{bmatrix}$
6	$\begin{bmatrix} 0.993 & 0.022 & -0.114 \\ -0.009 & 0.993 & 0.116 \\ 0.116 & -0.115 & 0.987 \end{bmatrix}$	$\begin{bmatrix} 0.993 & 0.022 & -0.114 \\ -0.009 & 0.993 & 0.116 \\ 0.116 & -0.115 & 0.987 \end{bmatrix}$	$\begin{bmatrix} 0.993 & 0.022 & -0.114 \\ -0.009 & 0.993 & 0.116 \\ 0.116 & -0.115 & 0.987 \end{bmatrix}$
7	$\begin{bmatrix} 0.885 & -0.170 & 0.433 \\ 0.199 & 0.980 & -0.022 \\ -0.421 & 0.106 & 0.901 \end{bmatrix}$	$\begin{bmatrix} 0.885 & -0.170 & 0.433 \\ 0.199 & 0.980 & -0.021 \\ -0.421 & 0.105 & 0.901 \end{bmatrix}$	$\begin{bmatrix} 0.885 & -0.170 & 0.433 \\ 0.199 & 0.980 & -0.021 \\ -0.421 & 0.105 & 0.901 \end{bmatrix}$
8	$\begin{bmatrix} 0.380 & 0.119 & 0.917 \\ 0.107 & 0.979 & -0.172 \\ -0.920 & 0.163 & 0.360 \end{bmatrix}$	$\begin{bmatrix} 0.380 & 0.119 & 0.917 \\ 0.107 & 0.979 & -0.172 \\ -0.920 & 0.163 & 0.360 \end{bmatrix}$	$\begin{bmatrix} 0.380 & 0.119 & 0.917 \\ 0.107 & 0.979 & -0.172 \\ -0.920 & 0.163 & 0.360 \end{bmatrix}$
9	$\begin{bmatrix} -0.484 & 0.030 & 0.875 \\ 0.145 & 0.988 & 0.046 \\ -0.863 & 0.149 & -0.482 \end{bmatrix}$	$\begin{bmatrix} -0.484 & 0.030 & 0.875 \\ 0.145 & 0.988 & 0.046 \\ -0.863 & 0.149 & -0.482 \end{bmatrix}$	$\begin{bmatrix} -0.484 & 0.030 & 0.875 \\ 0.145 & 0.988 & 0.046 \\ -0.863 & 0.149 & -0.482 \end{bmatrix}$
10	$\begin{bmatrix} -0.423 & 0.256 & 0.869 \\ 0.143 & 0.966 & -0.215 \\ -0.895 & 0.033 & -0.446 \end{bmatrix}$	$\begin{bmatrix} -0.423 & 0.256 & 0.869 \\ 0.143 & 0.966 & -0.215 \\ -0.895 & 0.033 & -0.446 \end{bmatrix}$	$\begin{bmatrix} -0.423 & 0.257 & 0.869 \\ 0.143 & 0.966 & -0.215 \\ -0.895 & 0.033 & -0.446 \end{bmatrix}$

Table D-3: The rotation matrices calculated using the two multiplicative decomposition combinations and using the standard method for cases 11-20.

Case	Rotation matrix following [Dynamic]*[Static]$^{-1}$	Rotation matrix following [Static]$^{-1}$*[Dynamic]	Rotation matrix following the standard method
11	$\begin{bmatrix} 0.993 & 0.099 & 0.063 \\ -0.108 & 0.982 & 0.152 \\ -0.047 & -0.158 & 0.986 \end{bmatrix}$	$\begin{bmatrix} 0.993 & 0.099 & 0.063 \\ -0.108 & 0.982 & 0.152 \\ -0.047 & -0.158 & 0.986 \end{bmatrix}$	$\begin{bmatrix} 0.993 & 0.099 & 0.063 \\ -0.108 & 0.982 & 0.152 \\ -0.047 & -0.158 & 0.986 \end{bmatrix}$
12	$\begin{bmatrix} -0.331 & 0.351 & 0.875 \\ 0.533 & 0.835 & -0.136 \\ -0.778 & 0.423 & -0.464 \end{bmatrix}$	$\begin{bmatrix} -0.330 & 0.353 & 0.875 \\ 0.533 & 0.835 & -0.136 \\ -0.779 & 0.422 & -0.464 \end{bmatrix}$	$\begin{bmatrix} -0.331 & 0.353 & 0.875 \\ 0.533 & 0.835 & -0.136 \\ -0.778 & 0.422 & -0.464 \end{bmatrix}$
13	$\begin{bmatrix} -0.133 & 0.234 & 0.963 \\ 0.416 & 0.895 & -0.160 \\ -0.899 & 0.380 & -0.216 \end{bmatrix}$	$\begin{bmatrix} -0.133 & 0.234 & 0.963 \\ 0.416 & 0.895 & -0.160 \\ -0.899 & 0.380 & -0.216 \end{bmatrix}$	$\begin{bmatrix} -0.133 & 0.234 & 0.963 \\ 0.416 & 0.895 & -0.160 \\ -0.899 & 0.380 & -0.216 \end{bmatrix}$
14	$\begin{bmatrix} 0.291 & 0.514 & 0.807 \\ -0.509 & 0.797 & -0.323 \\ -0.809 & -0.317 & 0.494 \end{bmatrix}$	$\begin{bmatrix} 0.292 & 0.513 & 0.807 \\ -0.510 & 0.797 & -0.322 \\ -0.809 & -0.318 & 0.494 \end{bmatrix}$	$\begin{bmatrix} 0.291 & 0.515 & 0.807 \\ -0.510 & 0.797 & -0.325 \\ -0.810 & -0.317 & 0.494 \end{bmatrix}$
15	$\begin{bmatrix} 0.149 & 0.344 & 0.926 \\ -0.041 & 0.938 & -0.342 \\ -0.987 & 0.013 & 0.154 \end{bmatrix}$	$\begin{bmatrix} 0.149 & 0.344 & 0.927 \\ -0.041 & 0.938 & -0.342 \\ -0.988 & 0.013 & 0.154 \end{bmatrix}$	$\begin{bmatrix} 0.149 & 0.347 & 0.926 \\ -0.041 & 0.938 & -0.345 \\ -0.988 & 0.013 & 0.154 \end{bmatrix}$
16	$\begin{bmatrix} 0.965 & 0.118 & 0.232 \\ -0.164 & 0.968 & 0.187 \\ -0.203 & -0.219 & 0.954 \end{bmatrix}$	$\begin{bmatrix} 0.965 & 0.118 & 0.232 \\ -0.164 & 0.968 & 0.187 \\ -0.203 & -0.219 & 0.954 \end{bmatrix}$	$\begin{bmatrix} 0.965 & 0.118 & 0.232 \\ -0.164 & 0.968 & 0.188 \\ -0.203 & -0.219 & 0.954 \end{bmatrix}$
17	$\begin{bmatrix} 0.536 & -0.308 & 0.786 \\ 0.487 & 0.873 & 0.010 \\ -0.690 & 0.378 & 0.618 \end{bmatrix}$	$\begin{bmatrix} 0.536 & -0.308 & 0.786 \\ 0.487 & 0.873 & 0.010 \\ -0.690 & 0.378 & 0.618 \end{bmatrix}$	$\begin{bmatrix} 0.536 & -0.308 & 0.786 \\ 0.487 & 0.873 & 0.010 \\ -0.690 & 0.378 & 0.618 \end{bmatrix}$
18	$\begin{bmatrix} -0.377 & -0.053 & 0.924 \\ -0.434 & 0.892 & -0.126 \\ -0.818 & -0.449 & -0.360 \end{bmatrix}$	$\begin{bmatrix} -0.377 & -0.053 & 0.924 \\ -0.434 & 0.892 & -0.126 \\ -0.818 & -0.449 & -0.360 \end{bmatrix}$	$\begin{bmatrix} -0.377 & -0.053 & 0.924 \\ -0.434 & 0.892 & -0.126 \\ -0.818 & -0.449 & -0.360 \end{bmatrix}$
19	$\begin{bmatrix} -0.082 & -0.264 & 0.961 \\ 0.443 & 0.854 & 0.272 \\ -0.893 & 0.448 & 0.047 \end{bmatrix}$	$\begin{bmatrix} -0.082 & -0.264 & 0.961 \\ 0.443 & 0.854 & 0.272 \\ -0.893 & 0.448 & 0.047 \end{bmatrix}$	$\begin{bmatrix} -0.082 & -0.265 & 0.961 \\ 0.443 & 0.854 & 0.273 \\ -0.893 & 0.448 & 0.047 \end{bmatrix}$
20	$\begin{bmatrix} -0.388 & 0.138 & 0.911 \\ -0.152 & 0.966 & -0.211 \\ -0.909 & -0.220 & -0.354 \end{bmatrix}$	$\begin{bmatrix} -0.388 & 0.138 & 0.911 \\ -0.152 & 0.966 & -0.211 \\ -0.909 & -0.220 & -0.354 \end{bmatrix}$	$\begin{bmatrix} -0.388 & 0.138 & 0.911 \\ -0.152 & 0.966 & -0.211 \\ -0.909 & -0.220 & -0.354 \end{bmatrix}$

Table D-4: Final shank positions calculated using the two multiplicative decomposition combinations and using the standard method.

Case	Shank final following [Dynamic]*[Static]$^{-1}$	Shank final following [Static]$^{-1}$*[Dynamic]	Shank final following the standard method
1	$[-0.997 \quad -0.054 \quad -0.058]$	$[-0.997 \quad -0.054 \quad -0.058]$	$[-0.997 \quad -0.054 \quad -0.058]$
2	$[-0.883 \quad 0.341 \quad 0.320]$	$[-0.884 \quad 0.339 \quad 0.320]$	$[-0.883 \quad 0.343 \quad 0.320]$
3	$[-0.140 \quad -0.072 \quad -0.987]$	$[-0.140 \quad -0.073 \quad -0.987]$	$[-0.140 \quad -0.073 \quad -0.987]$
4	$[-0.977 \quad -0.119 \quad 0.174]$	$[-0.977 \quad -0.120 \quad 0.174]$	$[-0.977 \quad -0.119 \quad 0.174]$
5	$[-0.869 \quad 0.095 \quad -0.485]$	$[-0.869 \quad 0.094 \quad -0.485]$	$[-0.869 \quad 0.094 \quad -0.485]$
6	$[0.114 \quad -0.116 \quad -0.987]$	$[0.114 \quad -0.116 \quad -0.987]$	$[0.114 \quad -0.116 \quad -0.987]$
7	$[-0.433 \quad 0.022 \quad -0.901]$	$[-0.433 \quad 0.021 \quad -0.901]$	$[-0.433 \quad 0.022 \quad -0.901]$
8	$[-0.917 \quad 0.172 \quad -0.359]$	$[-0.917 \quad 0.172 \quad -0.359]$	$[-0.917 \quad 0.172 \quad -0.359]$
9	$[-0.875 \quad -0.046 \quad 0.482]$	$[-0.875 \quad -0.046 \quad 0.482]$	$[-0.875 \quad -0.046 \quad 0.482]$
10	$[-0.869 \quad 0.215 \quad 0.446]$	$[-0.869 \quad 0.215 \quad 0.446]$	$[-0.869 \quad 0.216 \quad 0.446]$
11	$[-0.063 \quad -0.152 \quad -0.986]$	$[-0.063 \quad -0.152 \quad -0.986]$	$[-0.063 \quad -0.152 \quad -0.986]$
12	$[-0.875 \quad 0.133 \quad 0.464]$	$[-0.875 \quad 0.136 \quad 0.464]$	$[-0.875 \quad 0.134 \quad 0.464]$
13	$[-0.963 \quad 0.160 \quad 0.216]$	$[-0.963 \quad 0.160 \quad 0.216]$	$[-0.963 \quad 0.160 \quad 0.216]$
14	$[-0.807 \quad 0.323 \quad -0.494]$	$[-0.807 \quad 0.322 \quad -0.494]$	$[-0.807 \quad 0.325 \quad -0.494]$
15	$[-0.926 \quad 0.342 \quad -0.154]$	$[-0.927 \quad 0.342 \quad -0.154]$	$[-0.926 \quad 0.345 \quad -0.154]$
16	$[-0.232 \quad -0.187 \quad -0.954]$	$[-0.232 \quad -0.187 \quad -0.954]$	$[-0.232 \quad -0.188 \quad -0.954]$
17	$[-0.786 \quad -0.010 \quad -0.618]$	$[-0.786 \quad -0.010 \quad -0.618]$	$[-0.786 \quad -0.010 \quad -0.618]$
18	$[-0.924 \quad 0.126 \quad 0.360]$	$[-0.924 \quad 0.126 \quad 0.360]$	$[-0.924 \quad 0.126 \quad 0.360]$
19	$[-0.961 \quad -0.272 \quad -0.047]$	$[-0.961 \quad -0.272 \quad -0.047]$	$[-0.961 \quad -0.273 \quad -0.047]$
20	$[-0.911 \quad 0.211 \quad 0.354]$	$[-0.911 \quad 0.211 \quad 0.354]$	$[-0.911 \quad 0.211 \quad 0.354]$

Appendix E: Marker Set Information

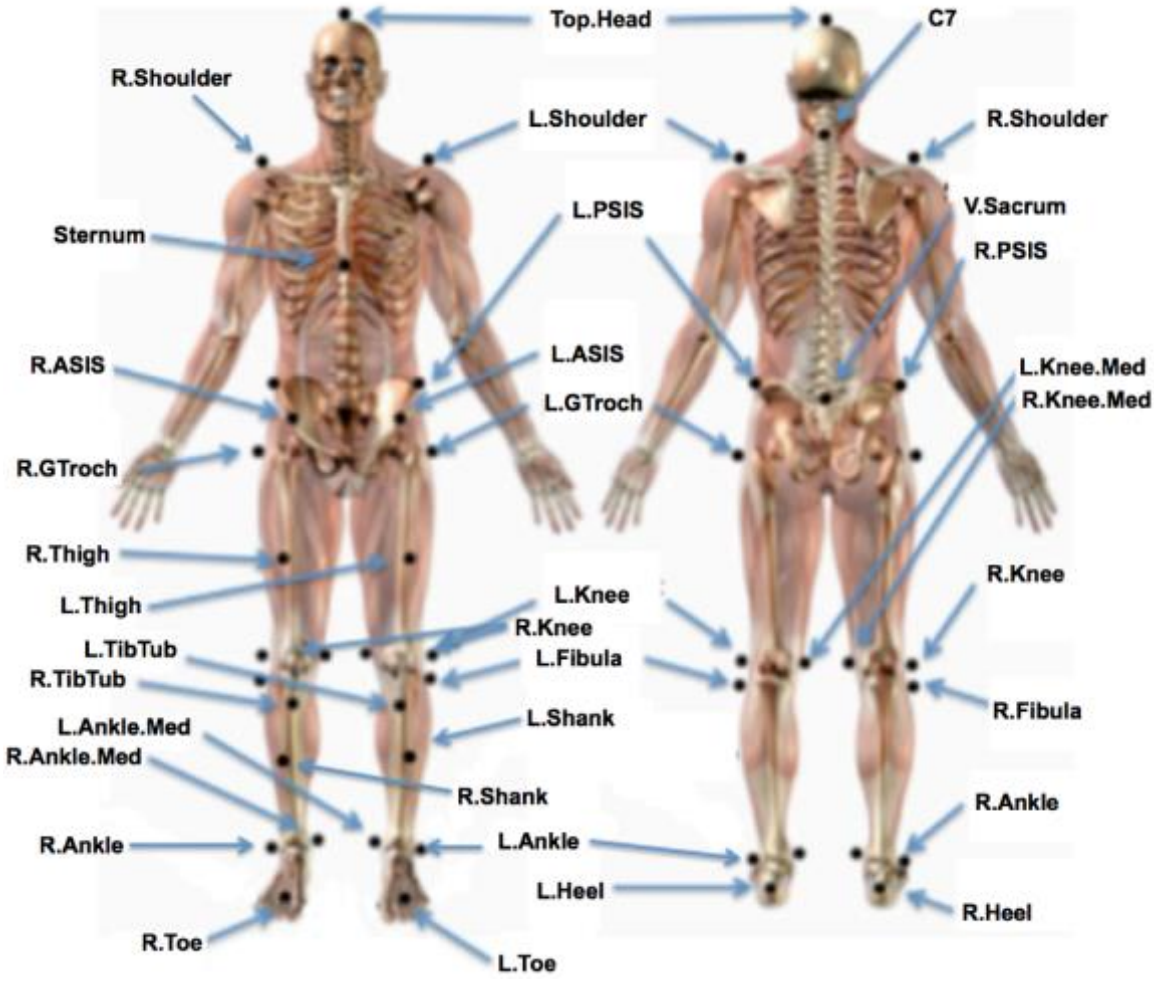

Figure E-1: Typical enhanced Helen Hayes marker set as used for the experiments.

Table E-1: A description of the markers placed on the subject according to an enhanced Helen Hayes markerset.

Marker	**Comments**
Top. Head	
Front. Head	
Rear. Head	
R. Acromion	
L. Acromion	
C7	
Sternum	
R. ASIS	
L. ASIS	
R. PSIS	
L. PSIS	
V. Sacral	
R. Thigh	
L. Thigh	
R. Knee	Lateral condyle of femur
L. Knee	Lateral condyle of femur
R. Fibula	
L. Fibula	
R. Tibial Tuberosity	
L. Tibial Tuberosity	
R. Shank	
L. Shank	
R. Ankle	Lateral condyle of fibula
L. Ankle	Lateral condyle of fibula
R. Heel	Posterior portion of calcaneus in line with R. Toe
L. Heel	Posterior portion of calcaneus in line with L. Toe
R. Toe	Distal end of 2nd metatarsal
L. Toe	Distal end of 2nd metatarsal
R. Knee Medial	Medial condyle of femur
L. Knee Medial	Medial condyle of femur
R. Ankle Medial	Medial condyle of fibula
L. Ankle Medial	Medial condyle of fibula

Appendix F: Non-Linear Solvers

The non-linear solvers used in this study operate by finding the value of the variables in a function to reduce the residuals of the objective function. This can be shown as:

$$\boldsymbol{F}(\boldsymbol{x}) = 0 \tag{11}$$

If an exact solution can't be found, then the solution which gives the lowest residual is selected as the solution. In some cases, the system of equations can be over constrained thus there's two solutions. In this case, a solution is picked by which values give the lowest residual.